Synthesis, Characterization, and Lewis-Acid Behaviour of $[W(NC_6F_5)F_4]_x$, and Computational Study of $W(NR)F_4$ (R = H, F, CH_3, CF_3, C_6H_5, C_6F_5), $W(NC_6F_5)F_4(NCCH_3)$, and $W(NC_6F_5)F_4(NC_5H_5)_n$ (n = 1, 2)

Douglas Turnbull[a,b], Stacey D. Wetmore[a,b], and Michael Gerken*[a,b]

[a]Canadian Centre for Research in Advanced Fluorine Technologies, University of Lethbridge, 4401 University Drive W, Lethbridge, AB, CA T1K 3M4

[b]Department of Chemistry and Biochemistry, University of Lethbridge, 4401 University Drive W, Lethbridge, AB, CA T1K 3M4

Abstract

Amorphous $[W(NC_6F_5)F_4]_x$ has been synthesized by the reaction of $[C_5H_5NH][W(NC_6F_5)F_5]$ with AsF_5 in CH_2Cl_2. The reaction of $[W(NC_6F_5)F_4]_x$ with CH_3CN yields monomeric $W(NC_6F_5)F_4(NCCH_3)$, whereas reaction with a sub-twofold excess of C_5H_5N in CH_3CN results in quantitative conversion to $W(NC_6F_5)F_4(NC_5H_5)$. Meanwhile, the reaction of $W(NC_6F_5)F_4(NCCH_3)$ with a large excess of C_5H_5N results in the precipitation of $W(NC_6F_5)F_4(NC_5H_5)_2$. These compounds have been characterized in the solid state by Raman spectroscopy and in solution by multinuclear NMR spectroscopy. The crystal structures of $W(NC_6F_5)F_4(NCCH_3)$ and $W(NC_6F_5)F_4(NC_5H_5)$, as well as improved structures of $WOF_4(NC_5H_5)_n$ (n = 1, 2) have been obtained at low temperatures. Furthermore, density-functional-theory (DFT-B3LYP) calculations have been conducted on the $W(NR)F_4$ (R = H, F, CH_3, CF_3, C_6H_5, C_6F_5) series as well as $W(NC_6F_5)F_4(NCCH_3)$ and $W(NC_6F_5)F_4(NC_5H_5)_n$ (n = 1, 2), providing optimized gas-phase geometries, vibrational frequencies, molecular orbitals, fluoride-ion affinities, and natural bond orbital (NBO) analyses.

1. Introduction

Tungsten oxide tetrafluoride, WOF_4, and its heavier congener WSF_4 are well understood to behave as Lewis acids and fluoride-ion acceptors. Existing as a fluorine-bridged tetramer[1] and chain polymer[2,3] in the solid state, respectively, their relatively weak fluorine-bridging interactions are easily cleaved upon reaction with a Lewis base (B) to afford monomeric adducts, $WChF_4(B)$ (Ch = O, S). In the case of WOF_4, numerous examples of adducts with oxygen,[4] nitrogen,[4–6] and phosphorus[7] bases have been isolated, as well as with KrF_2 and XeF_2.[8–10] Though studied to a lesser degree, WSF_4 has been demonstrated to form stable adducts with CH_3CN and C_5H_5N.[3,11] The related selenide, $WSeF_4$, has been isolated,[2,12] and though it has not been definitively characterized, there is preliminary evidence that its solid-state structure is analogous to WSF_4 and that it forms a monomeric adduct with CH_3CN.[12] In such adducts, the incoming Lewis base or fluorido ligand is invariably positioned trans to the chalcogen atom, which has been demonstrated unequivocally by several crystallographic and spectroscopic studies, initially of $[WOF_4]_4$.[1,13,14]

Salts of the $[WChF_5]^-$ and $[W_2Ch_2F_9]^-$ (Ch = O, S) anions have be prepared by the reaction of $WChF_4$ with fluoride-ion donors,[15–21] though $[WOF_5]^-$ and $[W_2O_2F_9]^-$ salts have alternatively been isolated upon the hydrolysis of WF_6 or the $[WF_7]^-$ anion.[16,22–27] The mixed $[W_2OSF_9]^-$ anion was formed in solution by the partial hydrolysis of the $[W_2S_2F_9]^-$ anion, or the deliberate reaction of $[WSF_5]^-$ with WOF_4, though it was found to exist only in admixture with the ternary $[W_2Ch_2F_9]^-$ anions *in situ* and could not be isolated.[21]

It was determined via competition reactions between WOF_4 and WSF_4 with F^- in CH_3CN that WOF_4 is the stronger of the two Lewis acids, which is attributed to the higher electronegativity of oxygen relative to sulfur. The oxide tetrafluoride is, in fact, a strong enough Lewis acid to form heptacoordinate adducts upon reaction with excess C_5H_5N[5] or with chelating diphosphines.[7] The

$[WOF_6]^{2-}$ anion has also been observed upon the reaction of WOF_4 with an excess of NOF[15] and by the hydrolysis of WF_6 in the presence of $N(C_2H_5)_3$.[28] An attempt to synthesize $WSF_4(NC_5H_5)_2$ was unsuccessful, and the optimization of a hypothetical geometry for this adduct (based on that known for $WOF_4(NC_5H_5)_2$)[5] resulted in dissociation into the 1:1 adduct and free C_5H_5N.[11]

The Lewis-acid and fluoride-ion-acceptor behaviour of analogous imido complexes ($W(NR)F_4$) is expected to be similar to that of WOF_4 and WSF_4, which has been verified indirectly by the preparation of a number of alkylimido complexes such as $W(NR)F_4(NCCH_3)$[29,30] and $[RNH_3][W(NR)F_5]$,[30–32] as well as various $[W(NCl)F_5]^-$,[33–35] $[W(NC_6F_5)F_5]^-$, and $[W_2(NC_6F_5)_2F_9]^-$ salts.[36] However, to the best of our knowledge, the only definitive example of a direct Lewis-acid-base reaction between $W(NR)F_4$ and a Lewis base is that of $W(NCl)F_4$ with CH_3CN to afford monomeric $W(NCl)F_4(NCCH_3)$, whose crystal structure revealed a stereochemistry similar to that of the $WChF_4$ adducts.[37] The parent compound was prepared by the direct fluorination of $W(NCl)Cl_4$ with F_2.

Herein, we report the synthesis of a new parent $W(NR)F_4$ compound, $[W(NC_6F_5)F_4]_x$, as well as its reactions with the nitrogen bases CH_3CN and C_5H_5N to afford $W(NC_6F_5)F_4(NCCH_3)$ and $W(NC_6F_5)F_4(NC_5H_5)_n$ (n = 1, 2). These species have been conclusively characterized, including crystal structures of $W(NC_6F_5)F_4(NCCH_3)$ and $W(NC_6F_5)F_4(NC_5H_5)$, and the Lewis acidity of $W(NC_6F_5)F_4$ is compared to those of WOF_4 and WSF_4. Furthermore, density-functional-theory (DFT-B3LYP) calculations have been performed on a series of monomeric $W(NR)F_4$ compounds (R = H, F, CH_3, CF_3, C_6H_5, C_6F_5) to compare their structural and electronic properties, including their fluoride-ion affinities (FIAs).

2. Results and Discussion

2.1. Syntheses and Properties of $[W(NC_6F_5)F_4]_x$, $W(NC_6F_5)F_4(NCCH_3)$, and $W(NC_6F_5)F_4(NC_5H_5)_n$ (n = 1, 2)

While the reaction of $[C_5H_5NH][W(NC_6F_5)F_5]$ with anhydrous HF resulted in partial fluoride-ion abstraction and the formation of $[C_5H_5NH][W_2(NC_6F_5)_2F_9]$,[36] introduction of the stronger fluoride-ion acceptor AsF_5 resulted in quantitative fluoride-ion abstraction, thereby affording a mixture of $[W(NC_6F_5)F_4]_x$ and $[C_5H_5NH][AsF_6]$ (Eq. 1). Neutral $[W(NC_6F_5)F_4]_x$ demonstrated high solubility in $CFCl_3$, resulting in deep orange-to-red solutions, and could subsequently be separated from the insoluble $[C_5H_5NH][AsF_6]$ by decantation. Removal of the $CFCl_3$ under dynamic vacuum yielded $[W(NC_6F_5)F_4]_x$ as transparent, red-orange shards. Despite their crystalline appearance, attempts at X-ray crystallography revealed that they were completely non-diffracting and $[W(NC_6F_5)F_4]_x$ prepared as such exists in an amorphous phase.

$$[C_5H_5NH][W(NC_6F_5)F_5] + AsF_5 \rightarrow 1/x[W(NC_6F_5)F_4]_x + [C_5H_5NH][AsF_6] \quad (1)$$

The dissolution of $[W(NC_6F_5)F_4]_x$ in CH_3CN resulted in an orange solution at −40 °C which lightened to yellow upon warming to ambient temperature over several minutes. Removal of CH_3CN under dynamic vacuum yielded $W(NC_6F_5)F_4(NCCH_3)$ as a microcrystalline, yellow solid (Eq. 2). The gradual dissipation of the orange colour in solution suggests that the solvolysis of $[W(NC_6F_5)F_4]_x$ by CH_3CN upon dissolution is not instantaneous. The CH_3CN adduct has been observed *in situ* by ^{19}F NMR spectroscopy upon solvolysis of the $[W_2(NC_6F_5)_2F_9]^-$ anion by CH_3CN.

$$1/x[W(NC_6F_5)F_4]_x + CH_3CN \xrightarrow{CH_3CN} W(NC_6F_5)F_4(NCCH_3) \quad (2)$$

Conversely, $[W(NC_6F_5)F_4]_x$ is only very slightly soluble in C_5H_5N at −35 °C, and dissolution could only be achieved at that temperature by the addition of CH_2Cl_2 as a co-solvent.

Upon removal of the volatile materials, yellow crystals of $W(NC_6F_5)F_4(NC_5H_5)$ were obtained, which could alternatively be prepared in quantitative yield by the reaction of $W(NC_6F_5)F_4$ with a sub-twofold excess of C_5H_5N in CH_3CN (Eq. 3). The dissolution of $W(NC_6F_5)F_4(NCCH_3)$ in a large (> 20-fold) excess of C_5H_5N at −35 °C instead resulted in a yellow-orange solution from which $W(NC_6F_5)F_4(NC_5H_5)_2$ promptly precipitated as an off-white powder that could not be dissolved upon warming to ambient temperature (Eq. 4). This 1:2 adduct is only very slightly soluble in CH_2Cl_2 and CH_3CN at low temperatures and attempts to warm the suspensions towards ambient temperature to increase solubility resulted in dissociation to the 1:1 adduct (Eq. 5). The formation of an isolable 1:2 adduct indicates that $W(NC_6F_5)F_4$ is qualitatively similar in Lewis acidity to WOF_4 and thus stronger than WSF_4.

$$1/x[W(NC_6F_5)F_4]_x + C_5H_5N \xrightarrow{CH_3CN} W(NC_6F_5)F_4(NC_5H_5) \quad (3)$$

$$W(NC_6F_5)F_4(NCCH_3) + 2C_5H_5N \xrightarrow{C_5H_5N} W(NC_6F_5)F_4(NC_5H_5)_2 + CH_3CN \quad (4)$$

$$W(NC_6F_5)F_4(NC_5H_5)_2 \rightarrow W(NC_6F_5)F_4(NC_5H_5) + C_5H_5N \quad (5)$$

Tungsten (pentafluorophenyl)imide tetrafluoride and its adducts with CH_3CN and C_5H_5N, though thermally stable in the solid state, are highly moisture sensitive; exposure to traces of moisture results in the formation of WOF_4 adducts or $[WOF_5]^-$ salts. The $W(NC_6F_5)F_4(NC_5H_5)_2$ adduct was observed to visibly decompose to an orange-brown material under an inert atmosphere of N_2 at ambient temperature over the course of months, likely due to dissociation to the 1:1 adduct. Like $WF_6(NC_5H_5)$ and its derivatives,[38] exposure of $W(NC_6F_5)F_4(NC_5H_5)_n$ (n = 1, 2) to HF results in cleavage of the W–N bond to yield $[C_5H_5NH][W(NC_6F_5)F_5]$.

2.2. Fluorine-19 NMR Spectroscopy

2.2.1. $[W(NC_6F_5)F_4]_x$

The ^{19}F NMR spectrum of $[W(NC_6F_5)F_4]_x$ in CH_2Cl_2 is complex (Figure 1), giving rise to a multitude of resonances within three distinct regions that range from 50 to 150 ppm, –60 to –120 ppm, and –140 to –160 ppm with relative integrations of 3:1:5. The first two regions are assigned to terminal (F_t) and bridging (F_b) fluorine-on-tungsten environments, respectively, within oligomeric and/or polymeric $[W(NC_6F_5)F_4]_x$. It appears that, like its oxide and sulfide analogs, $W(NC_6F_5)F_4$ aggregates via fluorine bridges such that the incoming fluorido ligand is exclusively positioned trans to the multiply bound ligand. This would explain the difference in chemical shift between the regions, as the imido ligand was observed to exhibit a strongly shielding trans influence in the $[W(NC_6F_5)F_5]^-$ and $[W_2(NC_6F_5)_2F_9]^-$ anions.[32,36]

The individual resonances within the fluorine-on-tungsten regions can differ in their relative integrations by several orders of magnitude, indicating that there is no single unique structure of $[W(NC_6F_5)F_4]_x$. Furthermore, though the lowest-frequency region is attributed to the C_6F_5 group, the signals are broad and the expected AA′MM′X spin system is not observed. This is attributed to the presence of large, slowly tumbling aggregate structure(s) in solution causing chemical-shift anisotropies and dipole-dipole interactions not to average out completely.

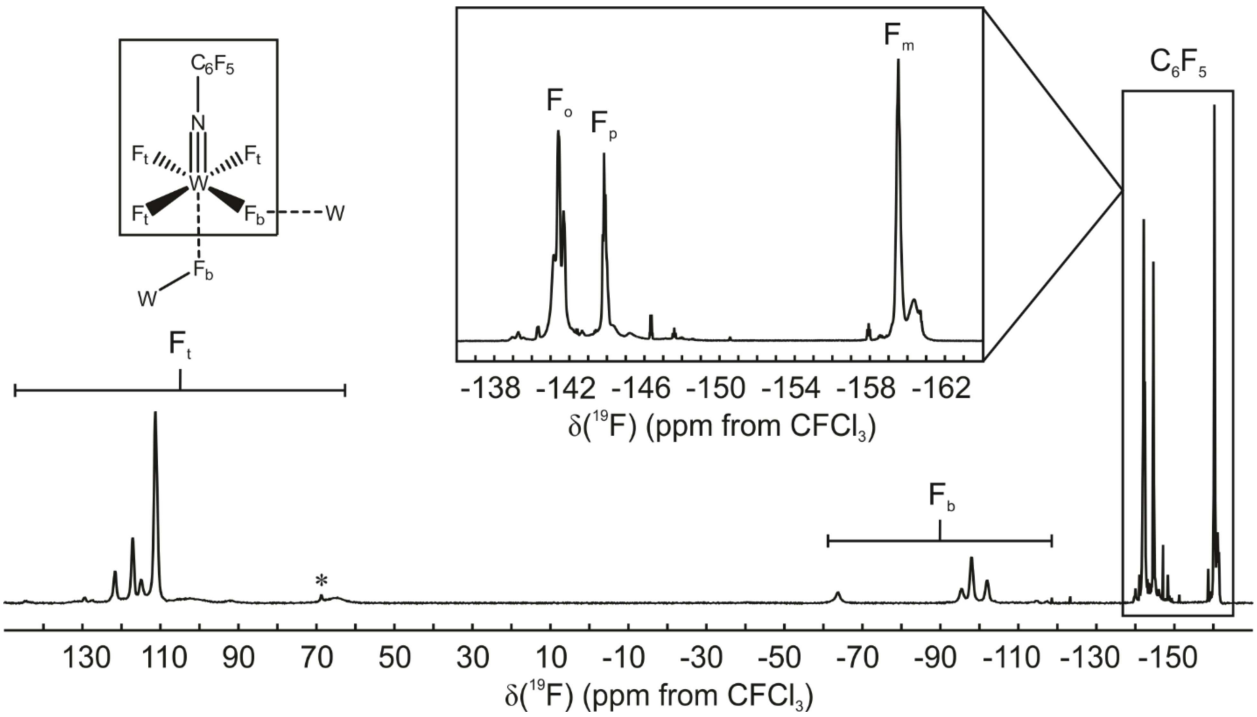

Figure 1. Fluorine-19 NMR spectrum (282.404 MHz) of $[W(NC_6F_5)F_4]_x$ recorded in CH_2Cl_2 at 20 °C. The asterisk (*) denotes an impurity of WOF_4.

2.2.2.$W(NC_6F_5)F_4(NCCH_3)$ and $W(NC_6F_5)F_4(NC_5H_5)$

The ^{19}F NMR spectra of the 1:1 adducts are simple in comparison to that of $[W(NC_6F_5)F_4]_x$ (Table 1). The fluorine-on-tungsten regions consist of singlets with ^{183}W satellites due to the chemical equivalence of the fluorido ligands, in excellent agreement with the previously reported spectroscopic data for $W(NC_6F_5)F_4(NCCH_3)$ (Figures S1 and S2 of the Supporting Information).[36] The chemical shifts of these singlets (59.14–61.57 ppm) are slightly lower than those reported for the analogous WOF_4 adducts (62.9–67.4 ppm)[4,5] and significantly lower than the WSF_4 adducts (81.8[11]–85.4[3] ppm). The fluorine-on-carbon environments consist of AA′MM′X spin systems that are highly characteristic of the NC_6F_5 moiety (Table 2 and depicted for $W(NC_6F_5)F_4(NC_5H_5)$ in Figure 2).[39]

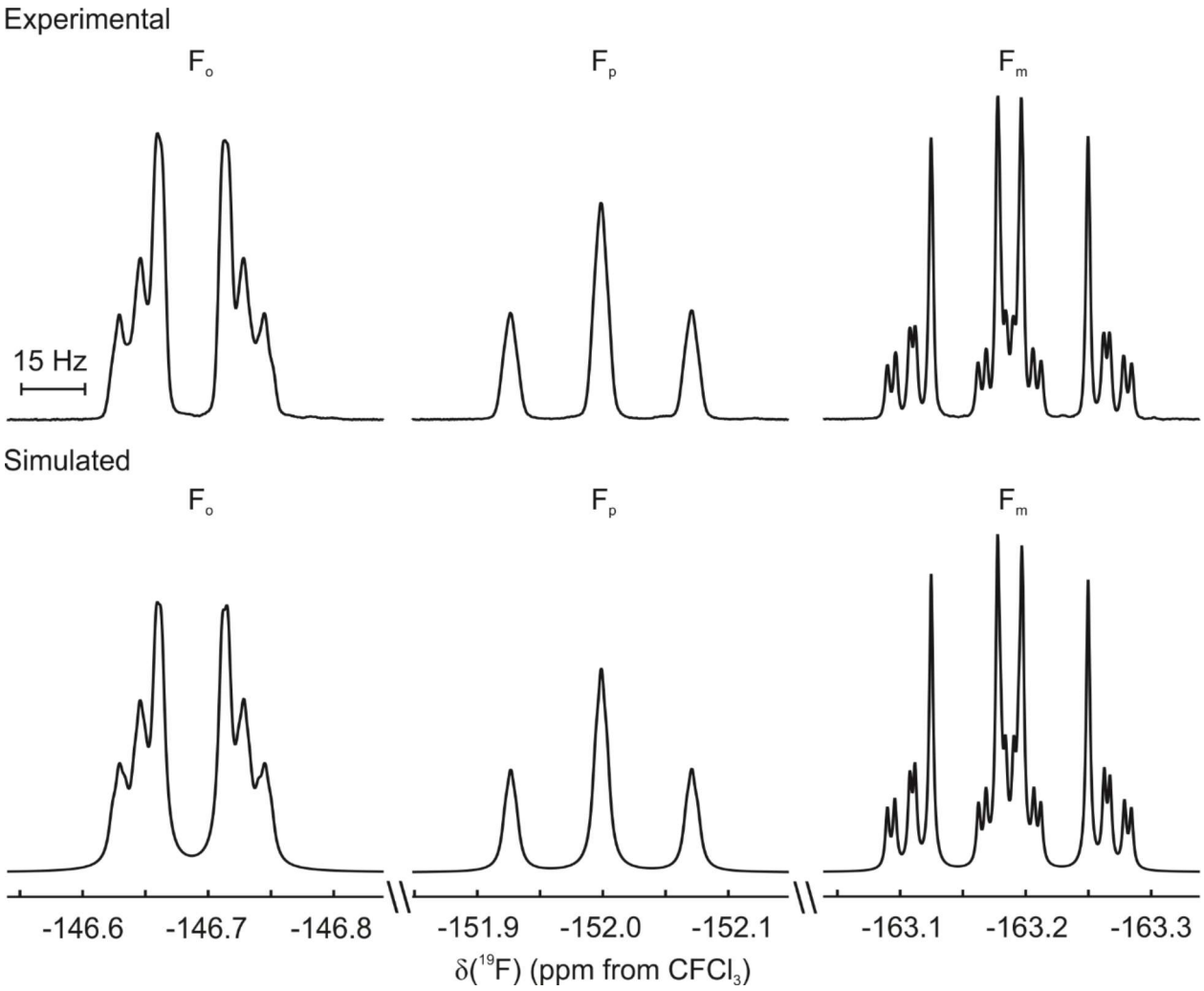

Figure 2. Experimental (top) and simulated (bottom) fluorine-on-carbon resonances in the ^{19}F NMR spectrum (282.404 MHz) of $W(NC_6F_5)F_4(NC_5H_5)$ recorded in CH_3CN at 20 °C. Spectral simulations were performed using MestreNova.

Table 1. Fluorine-19 NMR Spectroscopic Data for Fluorine-on-Tungsten Resonances of $W(NC_6F_5)F_4(NCCH_3)$ and $W(NC_6F_5)F_4(NC_5H_5)_n$ (n = 1, 2)

	$\delta(^{19}F)$ (ppm)[a]	J (Hz)			
		$^2J(F_A–F_M)$	$^2J(F_A–F_X)$	$^2J(F_M–F_X)$	$^1J(F–^{183}W)$
$W(NC_6F_5)F_4(NCCH_3)$[b]	61.57 (s)				38.3
$W(NC_6F_5)F_4(NC_5H_5)$[b]	59.14 (s)				35.5
$W(NC_6F_5)F_4(NC_5H_5)_2$[c]	–9.15 (F_A, t)		~55.5		
	–26.37 (F_M, dt)	53.5		83.9	
	–48.26 (F_X, dt)		57.3		

[a]Recorded at 282.404 MHz. Abbreviations denote singlet (s), triplet (t), and doublet of triplets (dt). [b]Recorded in CH_3CN at 20 °C. [c]Recorded in CH_2Cl_2 at –80 °C.

Table 2. Fluorine-19 NMR Spectroscopic Data for the Fluorine-on-Carbon Resonances of $W(NC_6F_5)F_4(NCCH_3)$ and $W(NC_6F_5)F_4(NC_5H_5)_n$ (n = 1, 2)

	$\delta(^{19}F)$ (ppm)[a]	J (Hz)[b]				
		$^3J(^{19}F–^{19}F_m)$	$^4J(^{19}F–^{19}F_p)$	$^4J(^{19}F–^{19}F')$	$^5J(^{19}F–^{19}F_m')$	$^1J(^{19}F–^{13}C)$
$W(NC_6F_5)F_4(NCCH_3)$[c]	−146.59 (F_o, m)	21.4		2.7	−6.4	n.o.[e]
	−151.35 (F_p, t)	20.4				n.o.[e]
	−162.85 (F_m, m)			2.0		n.o.[e]
$W(NC_6F_5)F_4(NC_5H_5)$[c]	−146.69 (F_o, m)	21.4	1.3	4.6	−6.5	253.1
	−152.00 (F_p, t)	20.3				257.2
	−163.19 (F_m, m)			1.4		250.1
$W(NC_6F_5)F_4(NC_5H_5)_2$[d]	−146.07 (F_o, dd)	~23			~6	~260
	−151.93 (F_p, t)	22.2				n.o.
	−162.36 (F_m, td)					n.o.

[a]Recorded at 282.404 MHz. Abbreviations denote triplet (t), doublet of doublets (dd), triplet of doublets (td), and multiplet (m). [b]$J(^{19}F–^{19}F)$ coupling constants were determined by spectral simulations using MestreNova. [c]Recorded in CH_3CN at 20 °C. [d]Recorded in CH_2Cl_2 at −80 °C. [e]Obscured by traces of NC_6F_5-containing impurities.

2.2.3. $W(NC_6F_5)F_4(NC_5H_5)_2$

Due to the prompt decomposition of $W(NC_6F_5)F_4(NC_5H_5)_2$ in solution at ambient temperature, its ^{19}F NMR spectra were recorded on a saturated CH_2Cl_2 solution at variable temperatures. At –80 °C, an A_2MX spin system is observed, which has been observed previously for $WOF_4(NC_5H_5)_2$ under similar conditions.[40] The observation of the same spin system in both adducts provides evidence that they share a common geometry, which is a pentagonal bipyramid in which the imido ligand occupies an axial position and the pyridyl ligands are in non-adjacent equatorial positions (Figure 3). Unlike in $WOF_4(NC_5H_5)_2$, the F_A resonance is a triplet rather than the expected doublet of doublets, due to the $^2J(F_A–F_M)$ and $^2J(F_A–F_X)$ coupling constants being of coincidentally similar magnitude (53.5 and 57.3 Hz; $\Delta J = 3.8$ Hz) and the linewidth ($\Delta\nu_{½} = 23$ Hz) not allowing for resolution of the individual couplings. No coupling to ^{183}W was observed for any of the three resonances. The ^1H and $^{13}C\{^1H\}$ NMR spectra each exhibit one set of resonances corresponding to the pyridyl ligands, corroborating their expected stereochemical equivalence (see the Experimental section).

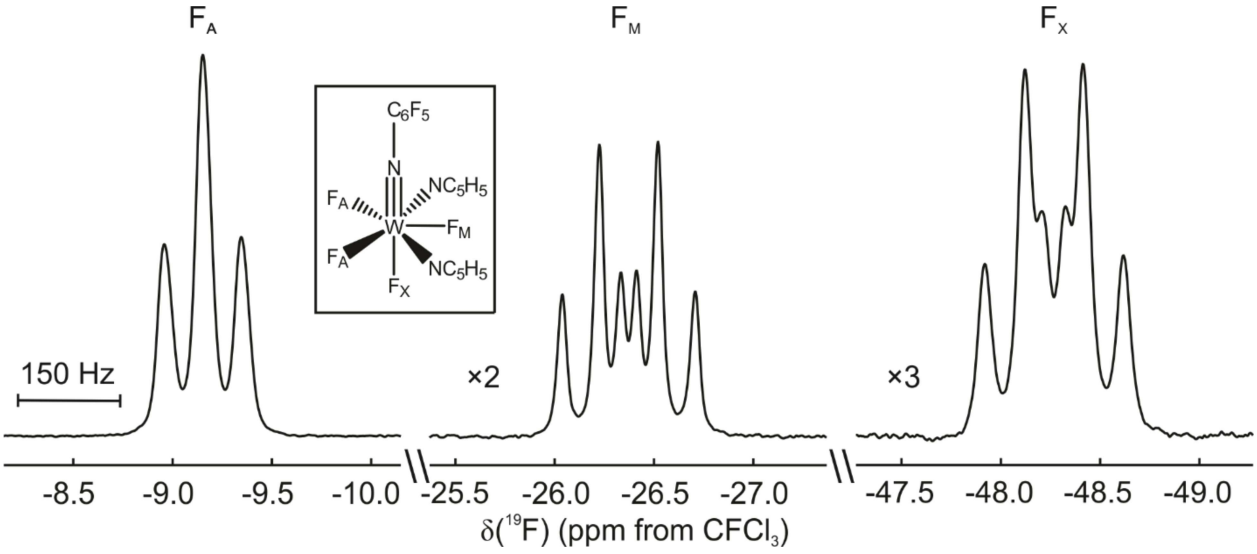

Figure 3. Fluorine-on-tungsten resonances in the ^{19}F NMR spectrum (282.404 MHz) of $W(NC_6F_5)F_4(NC_5H_5)_2$ recorded in CH_2Cl_2 at −80 °C.

Upon gradual warming to −20 °C, the F_A and F_M signals simplified to broad singlets and the F_X signal, formerly a doublet of triplets, became a quartet (Figure S3 of the Supporting Information). The axial ligand thus appears to remain rigid at this temperature, allowing it to couple to the now rapidly exchanging equatorial fluorido ligands ($^2J(F_{ax}–F_{eq})$ *ca.* 70 Hz). Above this temperature, irreversible decomposition began, and the adduct was observed to have dissociated almost entirely upon standing at 0 °C for less than five minutes. Regardless of temperature, the fluorine-on-carbon environment maintains the characteristic AA′MM′X spin system observed in the 1:1 adducts, though the signals are broadened such that that ^4J coupling could not be observed (Table 2).

2.3. Molecular Geometries

The structures of $W(NC_6F_5)F_4(NCCH_3)$, $W(NC_6F_5)F_4(NC_5H_5)$, and $WOF_4(NC_5H_5)_n$ (n = 1, 2) were elucidated by X-ray crystallography. In addition, gas-phase geometries were optimized for $W(NC_6F_5)F_4(NCCH_3)$ and $W(NC_6F_5)F_4(NC_5H_5)_n$ (n = 1, 2) using the B3LYP functional.

Selected crystallographic data collection and refinement parameters are provided in Table 3, in addition to selected experimental and calculated geometric parameters in Tables Table **4** and Table **5**.

Table 3. Crystallographic Data Collection and Refinement Parameters for $W(NC_6F_5)F_4(NCCH_3)$, $W(NC_6F_5)F_4(NC_5H_5)$, and $WOF_4(NC_5H_5)_n$ (n = 1, 2)

	$W(NC_6F_5)F_4(NCCH_3)$	$W(NC_6F_5)F_4(NC_5H_5)$	$WOF_4(NC_5H_5)_n$	
			$n = 1$	$n = 2$
Chemical formula	$C_8H_3F_9N_2W$	$C_{11}H_5N_2F_9W$	$C_5H_5F_4NOW$	$C_{10}H_{10}F_4N_2OW$
Formula weight	481.97	520.02	354.95	434.05
Temperature (°C)	−173	−173	−163	−163
Crystal system	triclinic	triclinic	orthorhombic	monoclinic
Space group	$P\bar{1}$	$P\bar{1}$	*Pbcn*	*C*2/*c*
a (Å)	5.0807(3)	8.0731(3)	14.0171(6)	8.2014(5)
b (Å)	7.5999(4)	9.1572(4)	7.5875(4)	11.1972(5)
c (Å)	16.0822(11)	9.1978(3)	14.8565(10)	13.5387(9)
α (°)	92.238(5)	86.670(3)		
β (°)	92.833(5)	87.048(3)		107.256(7)
γ (°)	90.040(4)	88.811(3)		
V (Å^3)	619.74(6)	677.82(5)	1580.05(15)	1187.33(13)
Z	2	2	8	4
R_1 [$I \geq 2\sigma(I)$][a]	0.0338	0.0136	0.0215	0.0208
wR_2 [$I \geq 2\sigma(I)$][b]	0.0848	0.0337	0.0394	0.0522
CCDC	1899538	1899539	1899540	1899541

[a] $R_1 = \sum||F_o| - |F_c||/\sum|F_o|$. [b] $wR_2 = [\sum[w(F_o^2 - F_c^2)^2]/\sum w(F_o^4)]^{1/2}$.

Table 4. Selected Experimental and Calculated[a] Bond Lengths (Å) and Angles (°) of $W(NCl)F_4(NCCH_3)$, $W(NC_6F_5)F_4(NCCH_3)$, and $W(NC_6F_5)F_4(NC_5H_5)_n$ (n = 1, 2)

	$W(NCl)F_4(NCCH_3)$	$W(NC_6F_5)F_4(NCCH_3)$		$W(NC_6F_5)F_4(NC_5H_5)_n$		
				n = 1		n = 2
	exptl[b]	exptl	calcd	exptl	calcd	calcd
W–F_{eq}	1.878(4)–1.894(4)	1.873(6)–1.880(6)	1.882–1.884	1.8767(14)–1.8836(14)	1.886–1.889	1.913–1.944
W–F_{ax}						1.946
W–N(1)	1.722(8)	1.728(6)	1.743	1.738(2)	1.752	1.782
W–N(2)	2.267(9)	2.278(6)	2.375	2.2854(19)	2.366	2.232
W–N(3)						2.237
W–N(1)–C(1)	178.6(6)[c]	174.7(4)	180.0	171.69(18)	180.0	178.9
N(1)–W–F_{eq}	98.6(3)–99.1(2)	98.2(3)–99.5(3)	100.0–100.3	96.51(8)–100.77(8)	99.6–99.9	92.3–96.8
N(1)–W–F_{ax}						174.1
N(1)–W–N(2)	179.9(4)	178.7(4)	180.0	175.74(8)	180.0	93.0
N(1)–W–N(3)						93.6
N(2)–W–N(3)						140.4

[b]Calculated using the B3LYP functional with the Stuttgart basis set augmented by one f-type polarization function (W; α_f = 0.823) and the cc-pVTZ (H, C, N, F) basis set. [b]From reference 37. [c]Defined as W–N(1)–Cl.

Table 5. Selected Bond Lengths (Å) and Angles (°) of $WOF_4(NC_5H_5)_n$ (n = 1, 2)[a]

	n = 1	n = 2
W–F_{eq}	1.859(3)–1.868(3)	1.9132(19)–1.917(2)
W–F_{ax}		1.834(2)[b]
W–O	1.690(3)	1.834(2)[b]
W–N	2.344(3)	2.223(2)
O–W–F_{eq}	98.45(15)–98.85(15)	86.80(7)–93.96(10)
O–W–F_{ax}		173.60(13)
O–W–N	179.73(16)	87.74(10)–90.25(10)
N–W–N^i		143.43(14)

[a]Symmetry transformation: i = 1 – x, y, 0.5 – z. [b]Equivalent due to 50/50 disorder between O and F(1).

2.3.1. $W(NC_6F_5)F_4(NCCH_3)$ and $W(NC_6F_5)F_4(NC_5H_5)$

Single crystals of $W(NC_6F_5)F_4(NCCH_3)$ and $W(NC_6F_5)F_4(NC_5H_5)$ were obtained from solutions of $W(NC_6F_5)F_4$ in CH_3CN and C_5H_5N/CH_2Cl_2, respectively, upon slow removal of the solvent at low temperature. They crystallize in the triclinic space group $P\bar{1}$ with two molecules per unit cell. The γ angle of unit cell in the CH_3CN adduct is approximately 90° and the crystal is consequently twinned by pseudomerohedry.

The geometries of the 1:1 adducts are highly comparable and consist of an octahedral coordination sphere about the tungsten center in which the nitrogen bases are coordinated trans to the imido ligand (Figure 4). The W–N(1)–C(1) angles of the CH_3CN and C_5H_5N adducts deviate from linearity by only 5.3 and 8.3°, respectively, suggesting significant triple-bond character in the W≡N bond of the imido ligand via donation of the lone pair on nitrogen to the electron-poor tungsten center.

The C_6F_5 groups adopt staggered conformations relative to the WF_4 moieties, and it is observed that the fluorido ligands deviate from the ideal WF_4 plane towards the nitrogen base (N(1)–W–F_{eq}: 96.51(8)–100.77(8)°) to a similar extent to the analogous WSF_4 adducts (99.05(5)–100.74(6) Å)[3,11] and $WOF_4(NC_5H_5)$ (98.43(15)–98.95(15) Å; *vide infra*). The W–N(1), W–F, and (where applicable) dative W−N(2) bond lengths do not differ significantly between the $W(NC_6F_5)F_4$ adducts nor from those of $W(NCl)F_4(NCCH_3)$[37] (Table 4) and the $[W(NC_6F_5)F_5]^-$ and $[W_2(NC_6F_5)_2F_9]^-$ anions.[36] The coordination environments about the tungsten centers are consistent with previously reported WOF_4[4–6,8] and WSF_4[3,11] adducts whose crystal structures have been elucidated.

The optimized gas-phase geometries of the adducts are in excellent agreement with the experimentally determined structures. They adopt (pseudo-)C_2-symmetric geometries with the

C_6F_5 groups staggered relative to the WF_4 moieties; while the C_5H_5N adduct conforms to the C_2 point group, the CH_3CN adduct is C_1-symmetric overall as a consequence of the local C_{3v} symmetry of the CH_3CN ligand. The only notable discrepancies are that the calculated W–N(2) bond lengths are somewhat overestimated (*ca*. 0.1 Å), as they were for $WSF_4(NCCH_3)$ (exptl.: 2.369(3); calcd.: 2.494 Å)[3] and $WSF_4(NC_5H_5)$ (exptl.: 2.319(2); calcd.: 2.439 Å)[11] at a similar level of theory. It should be noted that the dative W–N bonds of the $W(NC_6F_5)F_4$ adducts are calculated to differ by only 0.009 Å, which is consistent with the observed overlap of errors (within 2σ) in the experimentally determined W–N(2) bond lengths of the CH_3CN (2.278(6) Å) and C_5H_5N (2.2854(19) Å) adducts.

In the crystal structure of $W(NC_6F_5)F_4(NC_5H_5)$, the W–N(1)–C(1) (171.69(18)°) and N(1)–W–N(2) (175.74(8)°) angles deviate further from linearity than in the CH_3CN adduct. This likely arises from the antiparallel-displaced π-stacking interactions between adjacent molecules causing them to flex towards one another (Figure 4c). It appears that these interactions are facilitated via electron-poor C_6F_5 groups centering over the relatively electron-rich nitrogen atoms of adjacent pyridyl ligands. In contrast, crystal packing in the CH_3CN adduct is dominated by parallel-displaced π-stacking interactions along the *a* axis (Figure S4 of the Supporting Information). This distortion of the C(1)–N(1)–W–N(2) skeleton in the C_5H_5N adduct was not reproduced computationally, further suggesting that its origin lies in solid-state interactions.

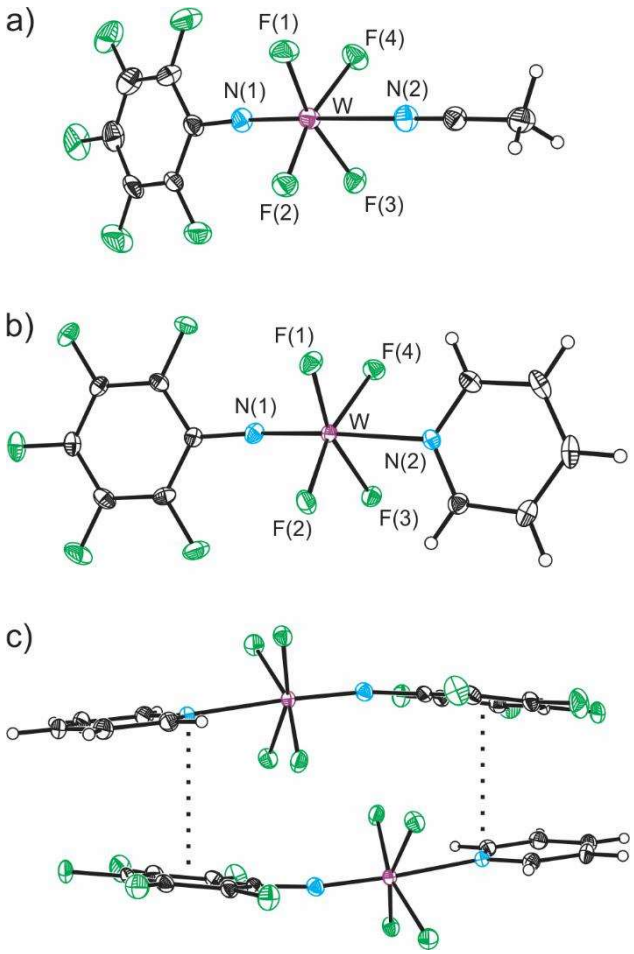

Figure 4. Thermal ellipsoid plots (50% probability level) of a) $W(NC_6F_5)F_4(NCCH_3)$ and b) $W(NC_6F_5)F_4(NC_5H_5)$ with c) intermolecular π-stacking interactions in the latter.

2.3.2. $W(NC_6F_5)F_4(NC_5H_5)_2$

Attempts to crystallize $W(NC_6F_5)F_4(NC_5H_5)_2$ from C_5H_5N and mixtures thereof with CH_3CN and CH_2Cl_2 did not return crystals suitable for X-ray crystallography, whereas when additional C_5H_5N was not present in the solvent, the 1:1 adduct crystallized instead. As such, in the absence of crystallographic data, the geometry of the 1:2 adduct was optimized based on that determined for $WOF_4(NC_5H_5)_2$ (Figure 5),[5,40] given the similarities between their low-temperature ^{19}F NMR spectra (*vide supra*). This pentagonal-bipyramidal geometry is ubiquitous in high-valent fluorido complexes of tungsten(VI) and rhenium(VII) containing multiply bound ligands, considering that the known heptacoordinate WOF_4 adducts,[5,7,40] as well as the $[WOF_6]^{2-}$[28] and $[ReOF_6]^-$[41] anions, have all been found to adopt such a geometry.

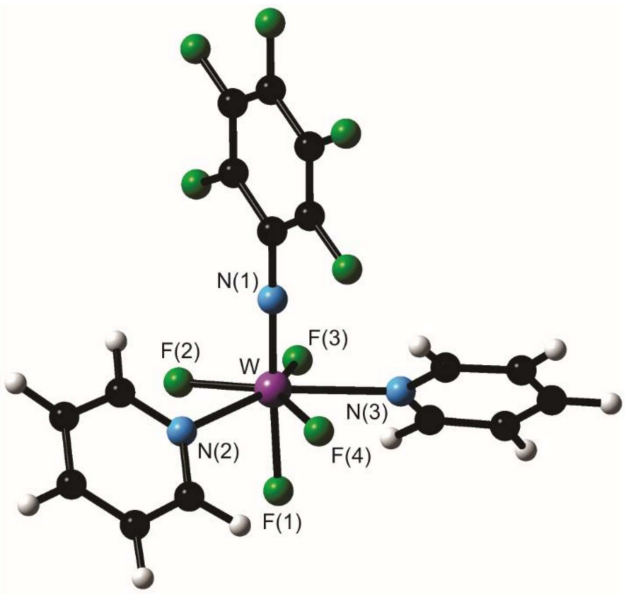

Figure 5. Optimized gas-phase geometry of $W(NC_6F_5)F_4(NC_5H_5)_2$.

Interestingly, while the W–N(1) and W–F bonds of $W(NC_6F_5)F_4(NC_5H_5)_2$ are significantly longer than those predicted for the 1:1 adducts, reflecting the decrease in covalent character of those bonds caused by the coordination of a second pyridyl ligand, the dative W–N bonds of the 1:2 adduct (2.332–2.337 Å) are significantly shorter than those calculated for $W(NC_6F_5)F_4(NC_5H_5)$ (2.366 Å). This is attributed to the trans influence of the imido ligand weakening the W–N(2) bond in the 1:1 adduct, which instead affects the W–F(1) bond in the 1:2 adduct.

2.3.3. $WOF_4(NC_5H_5)_n$ (n = 1, 2)

It was thought that salient inferences of the Lewis acidity of $W(NC_6F_5)F_4$ relative to WOF_4 and WSF_4 could be made by comparing the dative W–N bond lengths in the nitrogen-base adducts. Indeed, the significantly shorter bonds in $W(NC_6F_5)F_4(NCCH_3)$ (2.278(6) Å) and $W(NC_6F_5)F_4(NC_5H_5)$ (2.2854(19) Å) in comparison to the analogous WSF_4 adducts (2.369(3)[3] and 2.319(2)[11] Å, respectively) would suggest that $W(NC_6F_5)F_4$ is the stronger Lewis acid. Unfortunately, the large errors in the reported crystal structure of $WOF_4(NC_5H_5)$[5] precluded similar comparisons to WOF_4 and an improved crystal structure of the adduct was sought.

The crystallization of $WOF_4(NC_5H_5)$ (Figure 6a) from CH_2Cl_2 at –80 °C resulted in an orthorhombic phase (*Pcbn*), which is pseudoisomorphic with the closely related $WSF_4(NC_5H_5)$ adduct (*Pcba*).[11] This differs from the monoclinic space group ($P2_1/c$) assigned to the previously reported crystal structure, though the two adopt highly similar crystal-packing motifs (Figures S6 and S7 of the Supporting Information). The newly reported W=O (1.690(3) Å) and W–F (1.859(3)–1.868(3)) bond lengths are of substantially superior quality and are found to be insignificantly different from those of $WOF_4\{OP(C_6H_5)_3\}$ (W=O: 1.682(5); W–F: 1.857(3)–1.871(3) Å).[4] However, it was also observed that the W–N bond (2.344(3) Å) is, in fact, longer

than in the WSF_4 adduct (2.319(2) Å). This is despite WOF_4 being the demonstrably stronger Lewis acid,[21] vitiating the notion that the relative Lewis acidities of the parent compounds could be ascertained by comparisons of the dative W–N bond lengths in their C_5H_5N adducts.

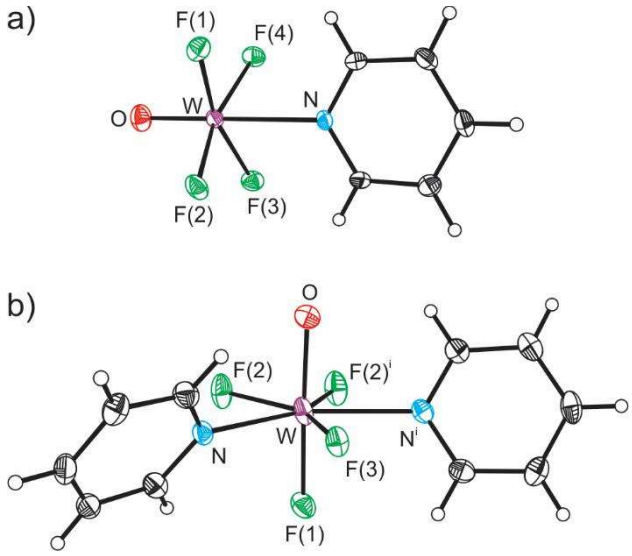

Figure 6. Thermal ellipsoid plots (50% probability level) of a) $WOF_4(NC_5H_5)$ and b) $WOF_4(NC_5H_5)_2$.

During our reinvestigation of the crystal structure of $WOF_4(NC_5H_5)$, crystals of $WOF_4(NC_5H_5)_2$ (Figure 6b) were fortuitously grown and thus studied by low-temperature X-ray crystallography. Due to the higher accuracy in the geometric parameters in both adducts, it was clearly observed that the W–F bonds were elongated upon coordination of the second pyridyl ligand, while the W–N bonds were significantly contracted (Table 5), as predicted in the optimized geometries of $W(NC_6F_5)F_4(NC_5H_5)_n$ (n = 1, 2). Despite the low temperature and improved quality

of the data, the axial O/F disorder in $WOF_4(NC_5H_5)_2$, which is imposed crystallographically by a twofold axis along the W–F(3) bond, could not be parsed.

2.4. Raman Spectroscopy

Raman spectra were recorded on solid samples of $[W(NC_6F_5)F_4]_x$, $W(NC_6F_5)F_4(NCCH_3)$, and $W(NC_6F_5)F_4(NC_5H_5)_n$ (n = 1, 2) at ambient temperature. Vibrational frequencies were calculated for the optimized geometries (*vide supra*), which resulted in excellent agreement between experimental and calculated data, and as such assignments were made on the basis of these calculations. In the case of $[W(NC_6F_5)F_4]_x$, the Raman spectrum was compared to the calculated vibrational frequencies of monomeric $W(NC_6F_5)F_4$, which agreed well with the experimental data. Selected vibrational frequencies are given in Table 6, and complete accounts of the vibrational spectroscopic data, with assignments, are provided in Tables S18–S21 and Figures S21–S24 of the Supporting Information.

Table 6. Selected Experimental and Calculated Frequencies (cm^{-1}) of $[W(NC_6F_5)F_4]_x$, $W(NC_6F_5)F_4(NCCH_3)$, and $W(NC_6F_5)F_4(NC_5H_5)_n$ (n = 1, 2)

	$\nu_s(WF_4)$		$\nu(WN(1))^a$		$\nu(WN(2))$	
	exptl[b]	calcd[c]	exptl[b]	calcd[c]	exptl[b]	calcd[c]
$[W(NC_6F_5)F_4]_x$ [d]	693(6)	698(29)	1373(17)	1384(70)		
$W(NC_6F_5)F_4(NCCH_3)$	676(6)	668(29)	1368(10)	1384(96)	224(2)	194(10)
$W(NC_6F_5)F_4(NC_5H_5)$	666(7) 642(4)	665(19) 649(23)	1359(19)	1381(152)	196(5)	187(9)
$W(NC_6F_5)F_4(NC_5H_5)_2$	585(5)[e]	605(25)[e]	1351(11)	1370(117)	190(2)	176(3)

[a]Highest frequency mode containing $\nu(WN(1))$ character, fully described as $\nu(WN(1) + C_oF_o + C_o'F_o' + C_pF_p)$. [b]Normalized Raman intensities are given in parentheses. [c]Calculated using the B3LYP functional with the Stuttgart basis set augmented by one f-type polarization function (W; α_f = 0.823) and the cc-pVTZ (H, C, N, F) basis set, unless otherwise noted. Absolute Raman intensities ($Å^4\ u^{-1}$) are given in parentheses. [d]Calculated for monomeric $W(NC_6F_5)F_4$ using the B3LYP functional with the Stuttgart basis set augmented by one f-type polarization function (W; α_f = 0.823) and the aug-cc-pVTZ (C, N, F) basis set. [e]Fully described as $\nu(WF(1) + WF(3) + WF(4))$; atoms are labelled as in Figure 5.

In the Raman spectra of $[W(NC_6F_5)F_4]_x$ and its derivative adducts (Figure 7), the bands corresponding to each $W(NC_6F_5)F_4$ moiety are highly similar to one another and to those reported previously for the $[W(NC_6F_5)F_5]^-$ and $[W_2(NC_6F_5)_2F_9]^-$ anions, both in frequency and relative intensity. This suggests that the vibrational coupling between the W≡N stretch in these species is identical to the anions, which was verified by the frequency calculations. In the Raman spectrum of $[W(NC_6F_5)F_4]_x$, one broad W–F stretching band is observed, as opposed to the numerous sharp W–F stretching bands of WOF_4 and WSF_4, likely due to the amorphous nature of the solid and the presence of a mixture of oligomeric and/or polymeric modifications.

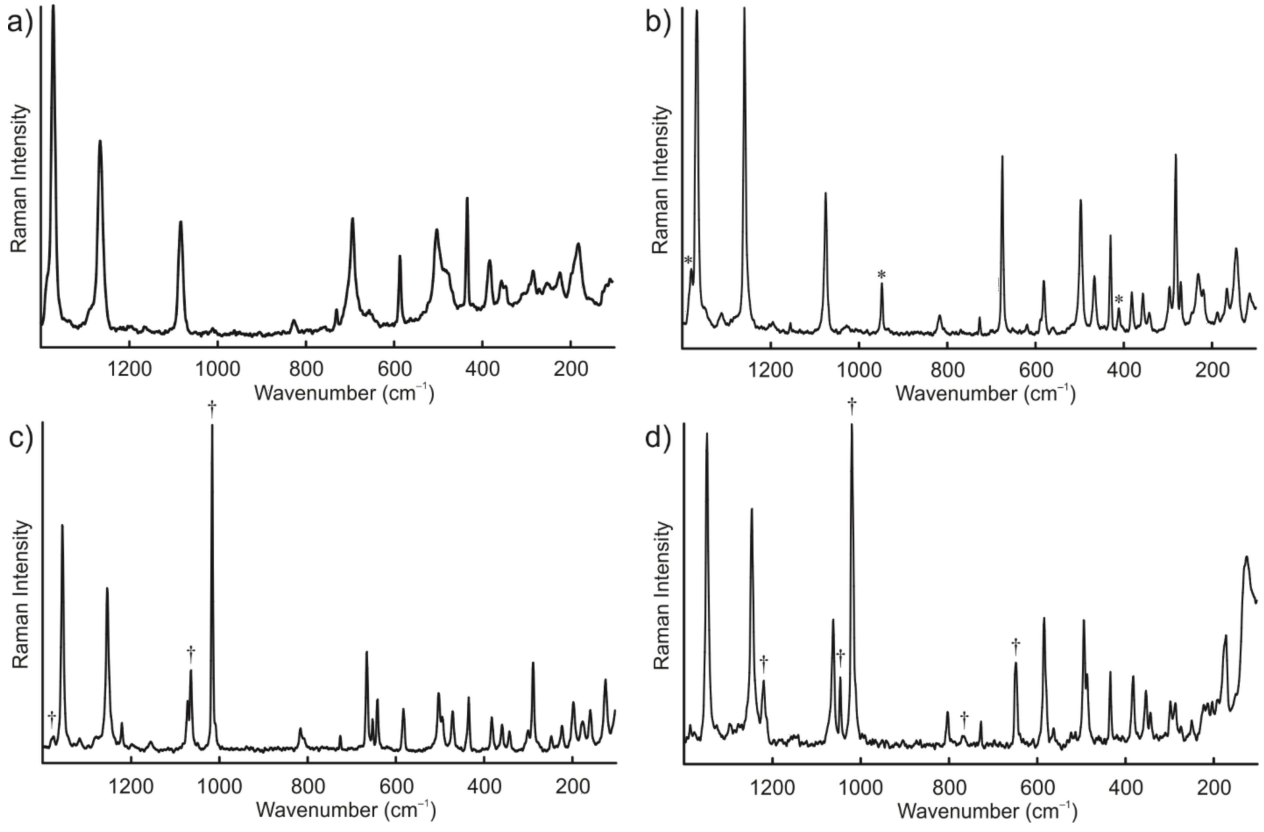

Figure 7. Raman spectra of a) $[W(NC_6F_5)F_4]_x$, b) $W(NC_6F_5)F_4(NCCH_3)$, c) $W(NC_6F_5)F_4(NC_5H_5)$, and d) $W(NC_6F_5)F_4(NC_5H_5)_2$, recorded at ambient temperature. Asterisks (*) and daggers (†) denote bands corresponding to the CH_3CN and C_5H_5N ligands, respectively.

The frequency of the symmetric W–F stretching mode correlates directly with the degree of electron donation from the nitrogen base(s) to the tungsten center. As such, the frequency of this band (in cm^{-1}) decreases in the series $[W(NC_6F_5)F_4]_x$ (693) > $W(NC_6F_5)F_4(NCCH_3)$ (676) > $W(NC_6F_5)F_4(NC_5H_5)$ (666/642) > $W(NC_6F_5)F_4(NC_5H_5)_2$ (585). The symmetric W–F stretching vibration of $W(NC_6F_5)F_4(NC_5H_5)$ is predicted to be split due to vibrational coupling to in-plane deformations of the pyridyl ligand, which agrees excellently with the observed splitting of the experimental Raman spectrum in this region.

In the cases of the adducts, there is also a complementary increase in frequency for characteristic bands corresponding to the nitrogen bases; in $W(NC_6F_5)F_4(NCCH_3)$, the C≡N stretching mode is shifted to 2328/2300 cm^{-1} from 2293/2253 cm^{-1} in free CH_3CN, whereas in the C_5H_5N adducts, the ring-breathing mode is shifted to 1018 (n = 1) and 1022 cm^{-1} (n = 2), respectively, from 990 cm^{-1} in free C_5H_5N (*cf.* $WOF_4(NC_5H_5)_n$: 1020 (n = 1) and 1022 cm^{-1} (n =2)).[5] The dative W–N stretching modes exhibit greater dependence on the size of the neutral ligand, and therefore the reduced mass of the vibration, than the strength of the bond, hence that of the CH_3CN adduct being higher in frequency than either C_5H_5N adduct; a similar phenomenon was observed for a series of WF_6 adducts with various pyridine derivatives.[38] Comparison of the C≡N stretching frequency (in cm^{-1}) in $W(NC_6F_5)F_4(NCCH_3)$ (2328/2300) with those determined previously for the analogous WOF_4 (IR: 2319)[4] and WSF_4 (Raman: 2313/2286)[3] adducts suggests again that $W(NC_6F_5)F_4$ is highly comparable in its Lewis acidity to WOF_4, and stronger than WSF_4.

Coupling is observed between the W≡N stretching vibration and various vibrations of the C_6F_5 group in manners identical to the $[W(NC_6F_5)F_5]^-$ and $[W_2(NC_6F_5)_2F_9]^-$ anions.[36] However, comparisons of the bands that possess W≡N stretching character reveal patterns in relative

frequency similar to, though lesser in magnitude than, that of the symmetric W–F stretching frequencies. It is possible that this trend arises due to weakening of the W≡N bond, but the significant degree of vibrational coupling obfuscates its true origin.

2.5. Computational Results

2.5.1. Optimized Geometries and Vibrational Frequencies of $W(NR)F_4$ (R = H, F, CH_3, CF_3, C_6H_5, C_6F_5)

Consistent with the experimentally determined structures of $WChF_4$ (Ch = O,[42] S,[43] Se[44]) in the gas phase, $W(NR)F_4$ (R = H, F, CH_3, CF_3, C_6H_5, C_6F_5) optimize to square-pyramidal geometries with the multiply bonded ligands occupying the apical positions. Selected geometric parameters are given in Table 7.

Potential-energy minima could not be found for $W(NCH_3)F_4$ or $W(NC_6H_5)F_4$, and the conformations that resemble those of their derivative $[W(NR)F_5]^-$ anions[36] exist as transition states for which the imaginary frequencies correspond to rotations of the R group relative to the WF_4 moiety. Potential-energy-surface scans of the rotation about the C–N bond revealed that there is a negligible energy barrier (<0.1 kJ mol^{-1}) and no obvious minimum, hence the difficulty in ascertaining the true ground-state geometries. In the case of $W(NC_6F_5)F_4$, while a ground-state geometry was found, it is not staggered and C_{2v}-symmetric like its derivative anion, but rather C_2-symmetric and nearly eclipsed in its conformation with a dihedral angle of 3.8° between the C_6F_5 group and the W–F(1) bond (Figure 8). Otherwise, the geometric parameters predicted for these compounds in the gas phase are highly similar to those calculated previously for the corresponding $[W(NR)F_5]^-$ anions.[36] The most prominent differences that arise upon removal of the axial fluorido ligand are slight contractions of the W≡N and W–F bonds and increases in the N≡W–F angles to better accommodate the mild steric repulsion between the imido and fluorido ligands.

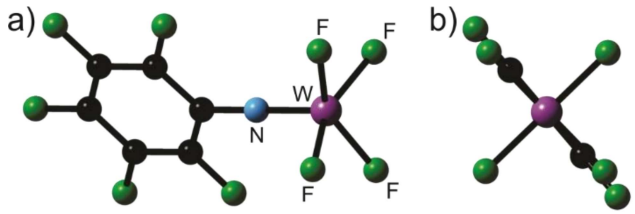

Figure 8. Optimized gas-phase geometry of $W(NC_6F_5)F_4$: a) side-on view, b) end-on view.

Table 7. Selected Calculated Bond Lengths (Å) and Angles (°) in $W(NR)F_4$ (R = H, F, CH_3, CF_3, C_6H_5, C_6F_5)[a]

R	W≡N	W–F	N≡W–F
H	1.713	1.869	105.4
F	1.719	1.870	105.2
CH_3	1.712	1.877	104.6–104.8
CF_3	1.727	1.861	105.3–105.5
C_6H_5	1.723	1.876	104.6
C_6F_5	1.731	1.863–1.874	103.2–106.7

[a]Calculated using the B3LYP functional with the Stuttgart basis set augmented by one f-type polarization function (W; $\alpha_f = 0.823$) and the aug-cc-pVTZ (H, C, N, F) basis set.

Their calculated vibrational spectra also exhibit characteristics much like those of their anionic counterparts, and the vibrational coupling of the W≡N stretch with vibrations of the R groups can be described in manners effectively identical to the anions. It is generally observed that the W≡N and W–F stretching modes increase in frequency upon removal of the axial fluorido ligand. This is evidenced most clearly in $W(NH)F_4$, for which the discrete W≡N and W–F stretches are shifted to 1080 and 704 cm^{-1}, respectively, from 967 and 639 cm^{-1} in the $[W(NH)F_5]^-$ anion. Vibrational frequencies, with complete assignments, for $W(NR)F_4$ (R = H, F, CH_3, CF_3, C_6H_5) are provided in Tables S13–S17 of the Supporting Information.

2.5.2. FIAs of $W(NR)F_4$ (R = H, F, CH_3, CF_3, C_6H_5, C_6F_5)

Given the difficulty in experimentally measuring the gas-phase FIAs of Lewis acids, which requires the generation of free F^- using an ion cyclotron resonance spectrometer, a reliable and accurate method for calculating the FIAs of main-group compounds was introduced by Christe, Dixon, and co-workers.[45] In this method, the pseudoisodesmic reactions of various Lewis acids (A) with the COF_3^- anion were studied (Eq. 6). The resulting reaction enthalpies, which can be considered the FIAs of A relative to COF_2, were then made absolute by adding the experimentally determined FIA of COF_2 (209 kJ mol^{-1}).[45]

$$A_{(g)} + COF_3^-{}_{(g)} \rightarrow AF^-{}_{(g)} + COF_{2(g)} \quad (6)$$

Herein, a similar approach is used in which the reaction of monomeric $W(NR)F_4$ with the $[WF_7]^-$ anion (Eq. 7) is considered. The resultant FIA of $W(NR)F_4$ relative to WF_6 is then corrected by the FIA of WF_6 (327 kJ mol^{-1}), previously calculated using ab initio (CCSD(T)) methods and corrected for zero-point energy and core-valence electron correlation, as well as relativistic and spin-orbit effects.[46] For these calculations, three geometries were predicted for the $[WF_7]^-$ anion using B3LYP: pentagonal-bipyramidal (D_{5h}), monocapped-octahedral (C_{3v}), and monocapped-trigonal-prismatic (C_{2v}). Of the three, the C_{2v}-symmetric geometry was the lowest in energy and was employed in the FIA determinations.

$$W(NR)F_{4(g)} + [WF_7]^-{}_{(g)} \rightarrow [W(NR)F_5]^-{}_{(g)} + WF_{6(g)} \quad (7)$$

It is evident from the range of calculated FIAs (Table 8) that the R group has drastic effects on the Lewis acidity of the tungsten centre, with the strongest Lewis acids possessing highly electron-withdrawing, fluorinated R groups. Coincidentally, the weakest Lewis acid of the series, $W(NCH_3)F_4$ (345 kJ mol^{-1}) is comparable in its strength to the archetypal Lewis acid BF_3 (344 kJ

mol^{-1}), whereas the strongest, $W(NCF_3)F_4$ (426 kJ mol^{-1}) approaches the strength of AsF_5 (443 kJ mol^{-1}).[45] The FIA of $W(NC_6F_5)F_4$ (411 kJ mol^{-1}) is predicted to be greater than those of WOF_4 (382 kJ mol^{-1}) and WSF_4 (362 kJ mol^{-1}). However, it should be noted that the C_6F_5 group is strongly π-accepting, complementing the π-donating behaviour of the incoming F^- and potentially favouring the formation of dative W–F bonds over other dative bonds to tungsten with predominantly σ character. As such, the expected superiority of $W(NC_6F_5)F_4$ as a fluoride-ion acceptor should not be generalized to all Lewis bases.

Table 8. Calculated FIAs (kJ mol^{-1}) of $W(NR)F_4$ (R = H, F, CH_3, CF_3, C_6H_5, C_6F_5) and $WChF_4$ (Ch = O, S)[a]

	FIA
$W(NH)F_4$	353
$W(NF)F_4$	417
$W(NCH_3)F_4$	345
$W(NCF_3)F_4$	426
$W(NC_6H_5)F_4$	367
$W(NC_6F_5)F_4$	411
WOF_4	382
WSF_4	362

[a]Calculated using the B3LYP functional with the Stuttgart basis set augmented by one f-type polarization function (W; $\alpha_f = 0.823$) and the aug-cc-pVTZ (H, C, N, O, F, S) basis set.

2.5.3. Molecular Orbitals

Selected MO energies for $W(NR)F_4$ are given in Table 9, which are depicted for $W(NC_6F_5)F_4$ in Figure 9. The HOMOs of $W(NR)F_4$ consist of the $d_{xz/yz}$–$p_{x/y}$ bonding interactions that comprise the W≡N π bonds, as do the HOMOs – 1 of $W(NCH_3)F_4$ and $W(NCF_3)F_4$ along with the HOMOs – 2 of $W(NC_6H_5)F_4$ and $W(NC_6F_5)F_4$. The HOMOs and HOMOs – 1 of the methyl derivatives are pseudodegenerate, whereas the HOMOs and HOMOs – 2 of the phenyl derivatives

are disparate due to highly different interactions of the inorganic moiety with delocalised σ and π systems in the R groups.

The LUMOs consist of π*(W–F) interactions involving the $d_{x^2-y^2}$ orbital on tungsten and do not contain any interaction between the WF_4 moieties and R groups. The nature of the LUMOs as such does not allow for appropriate orbital overlap with an incoming Lewis base. Instead, the LUMOs + 1, + 2, and + 3 incorporate the d_{xz}, d_{yz}, and d_{z^2} orbitals on tungsten such that they are available to accept electron density from either σ- (d_{z^2}) or π-donors (d_{xz} and d_{yz}). The π-accepting MOs are typically lower in energy with the notable exception of $W(NF)F_4$, which is attributed to the combined σ-withdrawing and π-donating properties of the nitrogen-bound fluorine atom. The "acidic" MOs are antibonding with respect to the W≡N and W–F bonds, consistent with the indiscriminate elongation of these bonds upon formation of the $[W(NR)F_5]^-$ anions.

Table 9. Selected MO Energies (eV) of $W(NR)F_4$ (R = H, F, CH_3, CF_3, C_6H_5, C_6F_5)[a,b]

R	HOMO – 2	HOMO – 1	HOMO	LUMO	LUMO + 1	LUMO + 2	LUMO + 3
H		–9.80		–3.76	–2.16 (π)		–1.82 (σ)
F		–9.63		–4.04	–3.45 (σ)	–2.28 (π)	
CH_3		–9.01[c]		–3.41	–1.77[c] (π)		–1.52 (σ)
CF_3		–10.33[c]		–4.34	–3.00[c] (π)		–2.41 (σ)
C_6H_5	–9.12		–7.31	–3.43	–2.51 (π)	–1.87 (π)	–1.49 (σ)
C_6F_5	–9.86		–7.84	–3.89	–3.20 (π)	–2.38 (π)	–2.06 (σ)

[a]Calculated using the B3LYP functional with the Stuttgart basis set augmented by one f-type polarization function (W; $\alpha_f = 0.823$) and the aug-cc-pVTZ (H, C, N, F) basis set. [b]Sigma (σ) and pi (π) denote the molecular-orbital character at the open coordination site of the tungsten center. [c]Molecular orbitals are pseudodegenerate due to the overall C_s symmetry of the compounds.

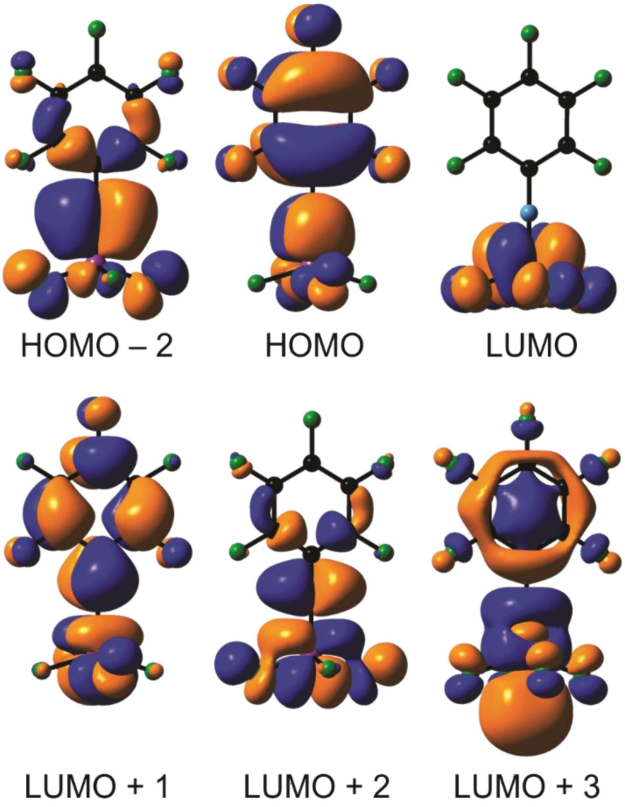

Figure 9. Selected MOs of $W(NC_6F_5)F_4$. Isosurface values are drawn at 0.02 e $Å^{-3}$.

2.5.4. Natural-Bond-Orbital (NBO) Analysis

Selected NPA charges on tungsten and Wiberg bond indices (WBIs) of the W≡N and W–F bonds are given in Table 10. It is observed that the WBIs of the W≡N bonds are found to be somewhat less than triple those of the W–F bonds, with the exception of $W(NH)F_4$, for which the ratio of WBIs is 3.0. The lowest ratios of WBIs are observed for $W(NCF_3)F_4$ (2.6) and $W(NC_6F_5)F_4$ (2.7) due to resonance of the W≡N bond with the strongly π-accepting R groups, which was described in detail previously for the $[W(NR)F_5]^-$ anions.[36]

Table 10. Selected NPA Charges and WBIs for $W(NR)F_4$ (R = H, F, CH_3, CF_3, C_6H_5, C_6F_5) and $W(NC_6F_5)F_4(L)_n$ (L = CH_3CN, C_5H_5N; n = 1, 2)[a]

R (nL)	Charge (W)	WBI		
		W≡N	W–F	W–N
H	+2.47	2.05	0.69	
F	+2.40	1.93	0.69	
CH_3	+2.44	2.03	0.67	
CF_3	+2.53	1.87	0.71–0.72	
C_6H_5	+2.44	1.93	0.68	
C_6F_5	+2.48	1.85	0.69–0.71	
C_6F_5 (CH_3CN)[b]	+2.28	1.84	0.69	0.21
C_6F_5 (C_5H_5N)[b]	+2.28	1.83	0.68–0.69	0.24
C_6F_5 ($2C_5H_5N$)[b]	+2.15	1.71	0.53–0.66	0.38

[a]Calculated using the B3LYP functional with the Stuttgart basis set augmented by one f-type polarization function (W; α_f = 0.823) and the aug-cc-pVTZ (H, C, N, F) basis set, unless otherwise noted. [b]Calculated using the B3LYP functional with the Stuttgart basis set augmented by one f-type polarization function (W; α_f = 0.823) and the cc-pVTZ (H, C, N, F) basis set.

In comparison to free, monomeric $W(NC_6F_5)F_4$, its 1:1 adducts possess less positively charged tungsten centers but no significant changes in the strengths of W–F and W≡N bonds. In the 1:2 adduct with C_5H_5N, however, marked decreases in the charge on the tungsten center and WBIs of the W≡N bond are observed. The most notable difference between the adducts is in the strength of the dative W–N bonds. The WBIs of these bonds in $W(NC_6F_5)F_4(NC_5H_5)_2$ (0.38) are comparable to that of $WF_6(NC_5H_5)$ (0.40),[38] and indicate a significant degree of covalent character. Meanwhile, those of the 1:1 adducts (0.21–0.24) are approximately one-third the WBIs of the W–F bonds (0.68–0.69), suggesting a greater degree of polarization towards the neutral ligands inflicted by the trans influence of the imido ligand. Comparison of NPA charges of the pyridyl ligands in the C_5H_5N adducts corroborate this notion, as the nitrogen atom (–0.50) and entire pyridyl ligand (+0.17) in the 1:1 adduct are less positively charged than in the 1:2 adduct (–0.43 and +0.25, respectively). This is further evidenced by the predicted contraction of the W–N bonds

upon coordination of a second pyridyl ligand (*vide supra*). Complete NPA charges, Wiberg valences, and WBIs are provided in Tables S22–S25 of the Supporting Information.

3. Conclusion

A synthetic route to $[W(NC_6F_5)F_4]_x$ via fluoride-ion abstraction from $[C_5H_5NH][W(NC_6F_5)F_5]$ has been developed. Though amorphous in the solid state, it is thought to aggregate by asymmetric fluorine bridges much like WOF_4 and WSF_4, forming various oligo- or polymeric modifications. In addition, it readily forms stable adducts upon reaction with CH_3CN and C_5H_5N. With C_5H_5N, a stable, heptacoordinate 1:2 adduct could be isolated, which was determined to adopt a pentagonal-bipyramidal geometry by ^{19}F NMR spectroscopy. These adducts have been comprehensively characterized in the solid state and in solution, and reveal that $W(NC_6F_5)F_4$ is a Lewis acid of similar strength to WOF_4. Lastly, DFT studies (B3LYP) of the $W(NR)F_4$ (R = H, F, CH_3, CF_3, C_6H_5, C_6F_5) series revealed that these compounds are expected to exhibit a range of Lewis acidities, with $W(NCH_3)F_4$ being the weakest in the series and $W(NCF_3)F_4$ the strongest. In particular, it was found that $W(NC_6F_5)F_4$ possesses a fluoride-ion affinity (411 kJ mol^{-1}) higher than those of WOF_4 (382 kJ mol^{-1}) and WSF_4 (362 kJ mol^{-1}).

4. Experimental

4.1. Materials and Apparatus

Caution! The high-valent fluorides WF_6 and AsF_5 are highly toxic and corrosive, rapidly evolving HF upon exposure to moisture, and appropriate safety measures should be taken during their handling.

All reactions were carried out in heat-sealed ¼”-o.d. FEP (tetrafluoroethene-hexafluoropropene copolymer) reactors that were connected to either stainless steel or Kel-F valves via flared fittings and prepassivated with 100% F_2. Volatile materials were distilled on a

Pyrex vacuum line equipped with glass valves fitted with 6-mm-o.d. PTFE stopcocks (J. Young), with the exceptions of WF_6 and AsF_5, which were distilled through a nickel/316 stainless steel vacuum line equipped with 316 stainless steel valves (Autoclave Engineers) and prepassivated with 100% F_2. Solid materials were handled in a drybox (Omni Lab, Vacuum Atmospheres) under an atmosphere of dry N_2.

Acetonitrile (Baker, 99.8%) was dried as described previously.[47] Pyridine (Sigma-Aldrich, 99.8%) was dried over CaH_2 and $CFCl_3$ (Aldrich, 99%) over P_4O_{10}; both were distilled prior to use. Dichloromethane was distilled from a solvent purification system (M. Braun MB-SPS) onto 4-Å molecular sieves and distilled once more onto fresh sieves. Tungsten hexafluoride (Ozark-Mahoning) was distilled prior to use. Arsenic pentafluoride,[48] $[C_5H_5NH][W(NC_6F_5)F_5]$,[36] and $WOF_4(NC_5H_5)_n$ (n = 1, 2)[5] were prepared according to the literature procedures.

4.2. Synthesis

4.2.1. $[W(NC_6F_5)F_4]_x$

In a typical synthesis, a ¼”-o.d. FEP reactor was charged with $[C_5H_5NH][W(NC_6F_5)F_5]$ (0.823 g, 1.52 mmol) in the dry box. Dichloromethane (1.327 g) was then distilled into the reactor at −196 °C and warmed to ambient temperature, resulting in an orange solution. Subsequently, AsF_5 (0.272 g, 1.60 mmol) was distilled into the reactor at −196 °C. Upon warming to −50 °C, the top of the CH_2Cl_2 solution, at its interface with AsF_5, turned dark red. The reactor was further warmed to ambient temperature and briefly agitated in an ultrasonic bath, resulting in a homogeneous orange suspension. The volatile materials were removed under dynamic vacuum at −65 °C for 2 h, at ambient temperature with constant agitation for 10 min, and at 45 °C for 20 min, affording a pale orange solid mixture along with a small amount of an involatile, yellow film that

coated the reactor walls (1.102 g, 1.08 g expected for 1:1 mixture of $[W(NC_6F_5)F_4]_x$ and $[C_5H_5NH][AsF_6]$).

The mixture was transferred into the side arm of a glass Y-shaped decanting vessel equipped with a PTFE valve (J. Young), and $CFCl_3$ (*ca.* 2 mL) was distilled onto the solid at −196 °C, resulting in the formation of a yellow solution above undissolved yellow-orange solid upon warming to ambient temperature, followed by agitating for several minutes. The solution was decanted into the straight arm of the decanting vessel, and the $CFCl_3$ was condensed back into the side arm at −10 °C, resulting in the solution in the straight arm becoming dark red. This was repeated five times, until only a faint yellow colour remained in the solution in the side arm. The solvent was then removed under dynamic vacuum at −80 °C for 1 h, and at ambient temperature for 45 min, affording $[W(NC_6F_5)F_4]_x$ (0.568 g, expected 0.672 g, 84.5% yield with respect to $[C_5H_5NH][W(NC_6F_5)F_5]$) as an orange solid in the straight arm and a mixture of white and yellow-orange solids in the side arm.

Due to the complicated nature of the ^{19}F NMR spectrum of $[W(NC_6F_5)F_4]_x$ in CH_2Cl_2, the purity of a sample was ascertained by ^{19}F NMR spectroscopy in CH_3CN, which typically gave rise to signals corresponding to $W(NC_6F_5)F_4(NCCH_3)$ along with impurities of $[C_5H_5NH][AsF_6]$ (3–4 mol%) and trace amounts of various imido- and oxidotungsten(VI) complexes including $WOF_4(NCCH_3)$, $[W_2(NC_6F_5)OF_9]^-$, and $[W_2(NC_6F_5)_2F_9]^-$.

4.2.2. $W(NC_6F_5)F_4(NCCH_3)$

In the dry box, a ¼”-o.d. FEP reactor was charged with $[W(NC_6F_5)F_4]_x$ (0.030 g, 0.068 mmol), onto which CH_3CN (0.123 g) was distilled at −196 °C. The reactor was warmed to −40 °C, resulting in an orange solution that lightened to yellow upon further warming to ambient temperature and letting stand for several minutes. The CH_3CN was removed under dynamic

vacuum at ambient temperature with constant agitation for 5 min, affording $W(NC_6F_5)F_4(NCCH_3)$ (0.033 g, expected 0.033 g) as a yellow, microcrystalline solid in quantitative yield.

$\delta(^1H)$ (ppm; CH_3CN, 20 °C, unlocked): 2.39 (CH_3).

4.2.3. $W(NC_6F_5)F_4(NC_5H_5)$

In the dry box, a ¼"-o.d. FEP reactor was charged with $[W(NC_6F_5)F_4]_x$ (0.062 g, 0.14 mmol), into which CH_3CN (0.206 g) was then distilled, resulting in an orange solution that lightened to yellow over the course of several minutes at ambient temperature. Subsequently, C_5H_5N (0.020 g, 0.25 mmol) was distilled into the reactor from a graduated glass weighing vessel. Upon warming the reactor to –40 °C and washing the C_5H_5N from the reactor walls with CH_3CN, the solution turned orange. The reactor was briefly warmed to ambient temperature and agitated to ensure reaction completion. Finally, the volatile materials were removed under dynamic vacuum at –40 °C for, at ambient temperature for 15 min, and at 45 °C for 1 h, affording $W(NC_6F_5)F_4(NC_5H_5)$ (0.072 g, expected 0.073 g) as an orange-brown powder in quantitative yield.

$\delta(^1H)$ (ppm; CH_3CN, 20 °C, unlocked): 8.77 (H_o, $^3J(H_o–H_m)$ = 6.5 Hz, $^4J(H_o–H_p)$ = 1.6 Hz); 8.16 (H_p, $^3J(H_p–H_m)$ = 7.7 Hz); 7.72 (H_m). $\delta(^{13}C\{^1H\})$ (ppm; CH_3CN, 20 °C, unlocked): 147.91 (C_o), 142.51 (C_p), 126.68 (C_m).

4.2.4. $W(NC_6F_5)F_4(NC_5H_5)_2$

Pyridine (0.206 g, 2.60 mmol) was distilled into a reactor containing freshly prepared $W(NC_6F_5)F_4(NCCH_3)$ (0.057 g, 0.12 mmol), after which the reactor was warmed to −40 °C and agitated for several minutes, resulting in a pale-orange suspension. The reactor was then warmed to ambient temperature and agitated briefly, before being cooled to −40 °C again. The volatile materials were removed under dynamic vacuum at −35 °C for 3 h, affording $W(NC_6F_5)F_4(NC_5H_5)_2$ (0.072 g, expected 0.071 g) as an off-white powder in quantitative yield.

δ(^{1}H) (ppm; CH_2Cl_2, –80 °C, unlocked): 7.86 (H_o, $^3J(H_o–H_m)$ = 5.7 Hz); 6.86 (H_p, $^3J(H_p–H_m)$ = 6.8 Hz); 6.44 (H_m). δ(^{13}C{^{1}H}) (ppm; CH_2Cl_2, –80 °C, unlocked): 147.57 (C_o), 144.57 (C_p), 125.29 (C_m).

4.3. X-ray Crystallography

4.3.1. Crystal Growth and Mounting

Yellow blocks of $W(NC_6F_5)F_4(NCCH_3)$ were grown from a solution of $[W(NC_6F_5)F_4]_x$ in CH_3CN (0.05 mL) by slow removal of the solvent under dynamic vacuum at –40 °C, and yellow plates of $W(NC_6F_5)F_4(NC_5H_5)$ were grown similarly from a solution of $[W(NC_6F_5)F_4]_x$ in C_5H_5N/CH_2Cl_2 (*ca.* 1:1; 0.1 mL) by slow removal of the solvent under dynamic vacuum at –35 °C. Colorless needles of $WOF_4(NC_5H_5)$ were grown by rapid cooling of a solution of $WOF_4(NC_5H_5)$ in CH_2Cl_2 to –80 °C and maintaining the solution at that temperature for 1 h, whereas colorless blocks of $WOF_4(NC_5H_5)_2$ were grown upon rapid cooling of a solution of $WOF_4(NC_5H_5)_2$ (which had previously been subjected to dynamic vacuum for 1 h at ambient temperature in an unsuccessful attempt at preparing $WOF_4(NC_5H_5)$) in CH_2Cl_2 to –20 °C and maintaining the solution at that temperature for 1 h.

The reactors containing the crystals were cut on an aluminium trough that was positioned close to the diffractometer and cooled to between –50 and −80 °C by a stream of cold, dry N_2. Once the crystals were deposited onto the trough, the selected crystal was affixed to a Nylon cryo-loop submerged in perfluorinated polyether oil (Fomblin Z-25) and quickly transferred to the goniometer.

4.3.2. Data Collection and Reduction

The crystals were centered on a Rigaku SuperNova diffractometer equipped with a Dectris Pilatus 3R 200K-A hybrid-pixel-array detector, a four-circle κ goniometer, an Oxford Cryostream

800, and sealed MoKα and CuKα X-ray sources. Data were collected using the MoKα source (λ = 0.71073 Å) between –163 °C and −173 °C. Crystals were screened for quality before a pre-experiment was run to determine the unit cell, and a data-collection strategy was calculated based on the determined unit cell and intensity of the preliminary data. This strategy was optimized to collect five-fold redundant data at a resolution of 0.77 Å. The data were processed using CrysAlisPro,[49] which applied necessary Lorentz and polarization corrections to the integrated data and scaled the data. A numerical (Gaussian-grid) absorption correction was generated based upon the indexed faces of the crystal. In the case of $W(NC_6F_5)F_4(NCCH_3)$, a twin component (rotated by 179.99° about [0 1 0] in the real lattice) was found using the Ewald reciprocal space viewer, resulting in two components in a ratio of 0.52:0.48. The data for these twin components were reduced separately.

4.3.3. Structure Solution and Refinement

Atom positions were determined using the intrinsic phasing method (ShelXT)[50] and were refined using least-squares refinement (ShelXL).[51] In the case of $W(NC_6F_5)F_4(NCCH_3)$, the data for the twin components were merged using ShelXL-97 merging weights and σ values as implemented in CrysAlisPro,[49] and the structure was solved using the merged data (HKLF 5 refinement). Non-hydrogen atoms were refined anisotropically and recommended weights for the atoms were determined before hydrogen atoms were introduced using a riding model (HFIX). The maximum and minimum electron density in the Fourier difference maps were located near the tungsten atom in all cases. Structure solution and refinement were performed with the aid of Olex2 (version 1.2).[52]

4.4. Raman Spectroscopy

Samples for Raman spectroscopy were prepared in flame-sealed glass m.p. capillaries at ambient temperature and recorded using a Bruker RFS-100 Raman spectrometer outfitted with a quartz beam-splitter and liquid-N_2-cooled germanium detector. The 1064-nm line of a Nd:YAG laser was used for excitation of the sample, and back-scattered (180°) radiation was sampled. The usable Stokes range of the collected data was 85 to 3500 cm^{-1} with a spectral resolution of 2 cm^{-1}. The laser power was typically set to 150 mW.

4.5. NMR Spectroscopy

Samples for NMR spectroscopy were prepared in heat-sealed 4-mm-o.d. FEP tubes sheathed in 5-mm-o.d. glass inserts, with the exception of that of $[W(NC_6F_5)F_4]_x$, which was prepared in a flame-dried, flame-sealed 5-mm-o.d. glass tube. Spectra were recorded using a Bruker Avance II 300 MHz spectrometer equipped with a 5-mm broadband probe and referenced externally to neat $CFCl_3$ (^{19}F) or $Si(CH_3)_4$ (^1H and $^{13}C\{^1H\}$) at 20 °C. Spectral simulations were performed using MestreNova.[53]

4.6. Computational Details

The DFT calculations were performed using the B3LYP functional as implemented in Gaussian 09 (revision D.01).[54] The Stuttgart basis set augmented by one f-type polarization function (α_f = 0.823)[55] and the associated pseudopotentials were used for tungsten. For the $W(NR)F_4$ series, the aug-cc-pVTZ basis set was employed for the first-, second-, and third-row elements. For the $W(NC_6F_5)F_4$ adducts, the cc-pVTZ basis set was used instead, as attempts to include diffuse functions resulted in SCF convergence failures. It has been found that the removal of diffuse functions resulted in only marginal differences in accuracy when employed in a comparative study on $WF_6(NC_5H_5)$.[38] The gas-phase geometries of WSF_4 and $[WSF_5]^-$ were

previously calculated at the same level of theory,[3,21] and were recalculated to obtain their energies and thermochemical data. Basis set parameters were obtained from the EMSL Basis Set Exchange.[56,57] Gas-phase geometry optimizations were performed using analytic-gradient methods, and all subsequent calculations were performed using the optimized geometries. Whenever possible, the experimental geometries were used as starting points for the geometry optimizations. The NBO analyses were performed using NBO (version 6.0),[58] and GaussView (version 5.0)[59] was used to visualize the vibrational modes and facilitate their description.

5. Acknowledgements

We would like to thank the National Science and Engineering Research Council of Canada for awarding Discovery grants to S.D.W. and M.G. as well as CGS-M and PGS-D scholarships to D.T. In addition, we would like to thank the University of Lethbridge for awarding the SGS Dean's Scholarship and Tuition Award to D.T. and supporting this work. The computational studies were performed using equipment funded through the Canada Foundation of Innovation, as well as resources made available through Westgrid and Compute/Calcul Canada.

6. References

(1) Edwards, A. J.; Jones, G. R. Fluoride crystal structures. Part I. Tungsten oxide tetrafluoride. *J. Chem. Soc. A* **1968**, 2074–2078.

(2) Holloway, J. H.; Kaučič, V.; Russell, D. R. Synthesis, chemistry, and crystal structures of high-valent transition-metal chalcogenide fluorides and their derivatives. *J. Chem. Soc., Chem. Commun.* **1983**, 1079–1081.

(3) Nieboer, J.; Hillary, W.; Yu, X.; Mercier, H. P. A.; Gerken, M. Syntheses, characterization, and computational study of WSF_4 and $WSF_4 \cdot CH_3CN$. *Inorg. Chem.* **2009**, *48* (23), 11251–11258.

(4) Levason, W.; Reid, G.; Zhang, W. Coordination complexes of the tungsten(VI) oxide fluorides WOF_4 and WO_2F_2 with neutral oxygen- and nitrogen-donor ligands. *J. Fluorine Chem.* **2016**, *184*, 50–57.

(5) Arnaudet, L.; Bougon, R.; Ban, B.; Charpin, P.; Isabey, J.; Lance, M.; Nierlich, M.; Vigner, J. Preparation, characterization, and crystal structure of the adducts $WOF_4 \cdot n C_5H_5N$ (n = 1, 2). *Inorg. Chem.* **1989**, *28* (2), 257–262.

(6) Arnaudet, L.; Bougon, R.; Ban, B.; Lance, M.; Nierlich, M.; Vigner, J. Preparation, characterization, and crystal structure of the tungsten hexafluoride and tetrafluoride oxide adducts $WF_6 \cdot$F-py and $WOF_4 \cdot$F-py (F-py = 2-fluoropyridine). *Inorg. Chem.* **1993**, *32* (7), 1142–1146.

(7) Emsley, J. W.; Levason, W.; Reid, G.; Zhang, W.; De Luca, G. Phosphine and diphosphine complexes of tungsten(VI) oxide tetrafluoride. *J. Fluorine Chem.* **2017**, *197*, 74–79.

(8) Tucker, P. A.; Taylor, P. A.; Holloway, J. H.; Russell, D. R.; IUCr. The adduct $XeF_2 \cdot WOF_4$. *Acta Crystallogr. B* **1975**, *31* (3), 906–908.

(9) Holloway, J. H.; Schrobilgen, G. J. Fluorine-19 and xenon-129 NMR studies of the $XeF_2 \cdot n WOF_4$ and $XeF_2 \cdot n MoOF_4$ (n = 1–4) adducts: Examples of nonlabile xenon-fluorine-metal bridges in solution. *Inorg. Chem.* **1980**, *19* (9), 2632–2640.

(10) Holloway, J. H.; Schrobilgen, G. J. Preparation and study by Raman spectroscopy of $KrF_2 \cdot MOF_4$, $XeF_2 \cdot MOF_4$, and $XeF_2 \cdot 2MOF_4$ (M = Mo, W) and a solution ^{19}F NMR study of $KrF_2 \cdot n MoOF_4$ (n = 1–3) and $KrF_2 \cdot WOF_4$. *Inorg. Chem.* **1981**, *20* (10), 3363–3368.

(11) Nieboer, J.; Yu, X.; Chaudhary, P.; Mercier, H. P. A.; Gerken, M. Synthesis, characterization, and computational study of $WSF_4 \cdot NC_5H_5$. *Z. Anorg. Allg. Chem.* **2012**, *638* (3–4), 520–525.

(12) Atherton, M. J.; Holloway, J. H. Preparation and characterisation of tungsten selenotetrafluoride, $WSeF_4$. *Inorg. Nucl. Chem. Lett.* **1978**, *14* (2–3), 121–123.

(13) Bennett, M. J.; Haas, T. E.; Purdham, J. T. Structure and bonding in the tungsten oxide tetrafluoride tetramer. *Inorg. Chem.* **1972**, *11* (1), 207–208.

(14) Asprey, L. B.; Ryan, R. R.; Fukushima, E. Structure of tungsten oxytetrafluoride. *Inorg. Chem.* **1972**, *11* (12), 3122–3122.

(15) Bougon, R.; Bui Huy, T.; Charpin, P. Acid properties of the oxytetrafluorides of molybdenum, tungsten, and uranium toward some inorganic fluoride ion donors. *Inorg. Chem.* **1975**, *14* (8), 1822–1830.

(16) Wilson, W. W.; Christe, K. O. Perfluoroammonium and cesium fluorotungstates. *Inorg. Chem.* **1981**, *20* (12), 4139–4143.

(17) Katayama, Y.; Hagiwara, R.; Ito, Y. Acid-base reactions of tungsten and uranium oxide fluorides in anhydrous hydrogen fluoride. *J. Fluorine Chem.* **1995**, *74* (1), 89–95.

(18) Mazej, Z.; Gilewski, T.; Goreshnik, E. A.; Jagličić, Z.; Derzsi, M.; Grochala, W. Canted antiferromagnetism in two-dimensional silver(II) bis[pentafluoridooxidotungstate(VI)]. *Inorg. Chem.* **2017**, *56* (1), 224–233.

(19) Atherton, M. J.; Holloway, J. H. Transition-metal thiofluorides: Preparation of WSF_4 and related anions. *J. Chem. Soc. Chem. Commun.* **1977**, 424.

(20) Hilbers, M.; Läge, M.; Mattes, R. Preparation and structure of $(Ph_3P)_2N[WSF_5]$. *Inorg. Chim. Acta* **1992**, *201* (1), 1–3.

(21) Nieboer, J.; Haiges, R.; Hillary, W.; Yu, X.; Richardet, T.; Mercier, H. P. A.; Gerken, M. Fluoride-ion acceptor properties of WSF_4: Synthesis, charcaterization, and computational study of the WSF_5^- and $W_2S_2F_9^-$ anions and ^{19}F NMR spectroscopic characterization of the $W_2O_SF_9^-$ anion. *Inorg. Chem.* **2012**, *51* (11), 6350–6359.

(22) Hargreaves, G. B.; Peacock, R. D. Higher complex fluorides of tungsten. *J. Chem. Soc.* **1958**, 2170–2175.

(23) Beuter, A.; Sawodny, W. Die schwingungsspektren und kraftkonstanten der anionen $MoOF_5^-$, $MoOF_5^{2-}$, MoF_6^-, und WOF_5^-. *Z. Anorg. Allg. Chem.* **1976**, *427* (1), 37–44.

(24) Massa, W.; Hermann, S.; Dehnicke, K. Reaktionen von chloronitrenkomplexen des molybdens und wolframs mit silberfluorid. Die kristallstruktur von $AsPh_4[WOF_5]$. *Z. Anorg. Allg. Chem.* **1982**, *493* (1), 33–40.

(25) Hoskins, B. F.; Linden, A.; O'Donnell, T. A. Controlled hydrolysis of the hexafluorides of molybdenum, tungsten and rhenium: Structure of oxonium (μ-fluoro)bis(tetrafluorooxotungstate(VI)). *Inorg. Chem.* **1987**, *26* (14), 2223–2228.

(26) Arnaudet, L.; Bougon, R.; Ban, B.; Lance, M.; Navaza, A.; Nierlich, M.; Vigner, J. Structure of the new fluoro complex of tungsten(VI): $[WF_4(bipy)_2]^{2+}\cdot 2[W_2O_2F_9]^-\cdot 0.25HF$ (bipy = 2,2′-bipyridyl). *J. Fluorine Chem.* **1992**, *59* (1), 141–152.

(27) Levason, W.; Monzittu, F. M.; Reid, G.; Zhang, W. Neutral and cationic tungsten(VI) fluoride complexes with tertiary phosphine and arsine coordination. *Chem. Commun.* **2018**, *54* (83), 11681–11684.

(28) Sakharov, S. G.; Kokunov, Y. V.; Gustyakova, M. P.; Buslaev, Y. A. Formation and structure of the $[WOF_6]^{2-}$ complex. *Dokl. Akad. Nauk SSSR* **1984**, *276* (1), 148–151.

(29) Harman, M.; Sharp, D. W. A.; Winfield, J. M. ^{1}H-^{14}N spin-spin coupling in methylimidotungsten(VI) tetrafluoride, acetonitrile. *Inorg. Nucl. Chem. Lett.* **1974**, *10* (2), 183–185.

(30) Chambers, O. R.; Harman, M.; Rycroft, D. S.; Sharp, D. W. A.; Winfield, J. M. Alkylimidotungsten(VI) fluorides. *J. Chem. Res.* **1977**, 1849–1876.

(31) Chambers, O. R.; Rycroft, D. S.; Sharp, D. W. A.; Winfield, J. M. Aminolysis reactions of tungsten hexafluoride: *N*-alkylimidofluorotungstates(VI). *Inorg. Nucl. Chem. Lett.* **1976**, *12* (7), 559–561.

(32) Fawcett, J.; Griffith, G. A.; Peacock, R. D.; Russell, D. R. The reaction between tungsten hexafluoride and pentafluoroaniline. *Polyhedron* **1988**, *7* (19), 2015–2022.

(33) Görge, A.; Dehnicke, K.; Fenske, D. Synthesis and crystal structure of [Na-15-crown-5][WF_5(NCl)]. *Z. Naturforsch. B* **1989**, *44* (2), 117–120.

(34) Stenger, H.; Dehnicke, K.; Hiller, W. [K(18-crown-6)][WF_5(NCl)]; Synthesis and crystal structure. *Z. Naturforsch. B* **1992**, *47* (7), 1054–1056.

(35) Dietrich, A.; Neumüller, B.; Dehnicke, K. Die kristallstruktur von K[$F_5W(\equiv NCl)$]. *Z. Anorg. Allg. Chem.* **2000**, *626* (12), 2443–2445.

(36) Turnbull, D.; Wetmore, S. D.; Gerken, M. Syntheses and characterization of $W(NC_6F_5)F_5^-$ and $W_2(NC_6F_5)_2F_9^-$ salts and computational sudies of the $W(NR)F_5^-$ (R = H, F, CH_3, CF_3, C_6H_5, C_6F_5) and $W_2(NC_6F_5)_2F_9^-$ anions. *Inorg. Chem.* **2017**, *56* (20), 12581–12593.

(37) Rhiel, M.; Wocadlo, S.; Massa, W.; Dehnicke, K. Reaktionen von $MoNCl_3$ und $WNCl_3$ mit elementarem fluor. Kristallstrukturen von [$MoO_2F_2(THF)_2$] und [WF_4(NCl)(CH_3CN)]. *Z. Anorg. Allg. Chem.* **1996**, *622* (7), 1195–1199.

(38) Turnbull, D.; Kostiuk, N.; Wetmore, S. D.; Gerken, M. Syntheses, characterisation, and computational studies of tungsten hexafluoride adducts with pyridine and its derivatives. *J. Fluorine Chem.* **2018**, *215*, 1–9.

(39) Hogben, M. G.; Graham, W. A. G. Chemical shifts and coupling constants in pentafluorophenyl derivatives. I. Correlations of chemical shifts, coupling constants, and π-electronic interactions. *J. Am. Chem. Soc.* **1969**, *91* (2), 283–291.

(40) Arnaudet, L.; Bougon, R.; Buu, B. Molecular structure of the $WOF_4 \cdot 2py$ (py = pyridine) adduct as refined by ^{19}F NMR spectroscopy. *J. Fluorine Chem.* **1995**, *74* (2), 223–225.

(41) Giese, S.; Seppelt, K. Structural principles in seven-coordinate subgroup compounds: The complex anions MoF_7^-, WF_7^-, and $ReOF_6^-$. *Angew. Chem. Int. Ed. Engl.* **1994**, *33* (4), 461–463.

(42) Robiette, A. G.; Hedberg, K.; Hedberg, L. Gas-phase electron diffraction study of the molecular structure of tungsten oxytetrafluoride, WOF_4. *J. Mol. Struct.* **1977**, *37* (1), 105–112.

(43) Rice, D. A.; Hagen, K.; Hedberg, L.; Hedberg, K.; Staunton, G. M.; Holloway, J. H. Gas-phase electron-diffraction study of tetrafluorosulfidotungsten(VI). *Inorg. Chem.* **1984**, *23* (13), 1826–1828.

(44) Hagen, K.; Rice, D. A.; Holloway, J. H.; Kaučič, V. Gas-phase electron diffraction study of Tetrafluoro(seleno)tungsten(VI), $WSeF_4$. *J. Chem. Soc., Dalt. Trans.* **1986**, 1821–1823.

(45) Christe, K. O.; Dixon, D. A.; McLemore, D.; Wilson, W. W.; Sheehy, J. A.; Boatz, J. A. On a quantitative scale for Lewis acidity and recent progress in polynitrogen chemistry. *J. Fluorine Chem.* **2000**, *101* (2), 151–153.

(46) Craciun, R.; Picone, D.; Long, R. T.; Li, S.; Dixon, D. A.; Peterson, K. A.; Christe, K. O. Third row transition metal hexafluorides, extraordinary oxidizers, and Lewis acids: Electron affinities, fluoride affinities, and heats of formation of WF_6, ReF_6, OsF_6, IrF_6, PtF_6, and AuF_6†. *Inorg. Chem.* **2010**, *49* (3), 1056–1070.

(47) Winfield, J. M. Acetonitrile, a convenient solvent for inorganic fluorides. *J. Fluorine Chem.* **1984**, *25* (1), 91–98.

(48) Emara, A. A. A.; Lehmann, J. F.; Schrobilgen, G. J. A laboratory-scale synthesis of high-purity AsF_5 by direct fluorination of AsF_3. *J. Fluorine Chem.* **2005**, *126* (9–10), 1373–1376.

(49) CrysAlisPro. Agilent Technologies, Ltd.: Yarnton, Oxfordshire, England 2014.

(50) Sheldrick, G. M. ShelXT. University of Göttingen: Göttingen, Germany 2015.

(51) Sheldrick, G. M. ShelXL. University of Göttingen: Göttingen, Germany 2015.

(52) Dolomanov, O. V.; Bourhis, L. J.; Gildea, R. J.; Howard, J. A. K.; Puschmann, H. Olex2. OlexSys Ltd., Durham University: Durham, England 2017.

(53) MestreNova. Mestrelab Research S.L.: Santiago de Compostela, Spain 2014.

(54) Frisch, M. J.; Trucks, G. W.; Schlegel, H. B.; Scuseria, G. E.; Robb, M. A.; Cheeseman, J. R.; Scalmani, G.; Barone, V.; Petersson, G. A.; Nakatsuji, H.; et al. Gaussian 09, Revision D.01. Gaussian, Inc.: Wallingford, CT, 2016.

(55) Ehlers, A. W.; Böhme, M.; Dapprich, S.; Gobbi, A.; Höllwarth, A.; Jonas, V.; Köhler, K. F.; Stegmann, R.; Veldkamp, A.; Frenking, G. A set of f-polarization functions for pseudo-potential basis sets of the transition metals Sc-Cu, Y-Ag, and La-Au. *Chem. Phys. Lett.* **1993**, *208* (1–2), 111–114.

(56) Feller, D. The role of databases in support of computational chemistry calculations. *J. Comput. Chem.* **1996**, *17* (13), 1571–1586.

(57) Schuchardt, K. L.; Didier, B. T.; Elsethagen, T.; Sun, L.; Gurumoorthi, V.; Chase, J.; Li, J.; Windus, T. L. Basis Set Exchange: A community database for computational sciences. *J. Chem. Inf. Model.* **2007**, *47* (3), 1045–1052.

(58) Glendening, E. D.; Badenhoop, J. K.; Reed, A. E.; Carpenter, J. E.; Bohmann, J. A.; Morales, C. M.; Landis, C. R.; Weinhold, F. NBO. Theoretical Chemistry Institute, University of Wisconsin: Madison, WI, USA 2013.

(59) GaussView. Gaussian, Inc.: Wallingford, CT, USA 2016.

Table of Contents Sypnosis and Graphic

Fluorine-bridged $[W(NC_6F_5)F_4]_x$ has been synthesized and found to form monomeric 1:1 adducts upon reaction with CH_3CN and C_5H_5N (see Figure). The $W(NC_6F_5)F_4(NCCH_3)$ adduct can be reacted with an excess of C_5H_5N to form heptacoordinate $W(NC_6F_5)F_4(NC_5H_5)_2$. In addition, the monomeric $W(NR)F_4$ (R = H, F, CH_3, CF_3, C_6H_5, C_6F_5) series, as well as the aforementioned adducts, have been studied computationally (B3LYP) to elucidate their structural, electronic, and Lewis-acid properties.

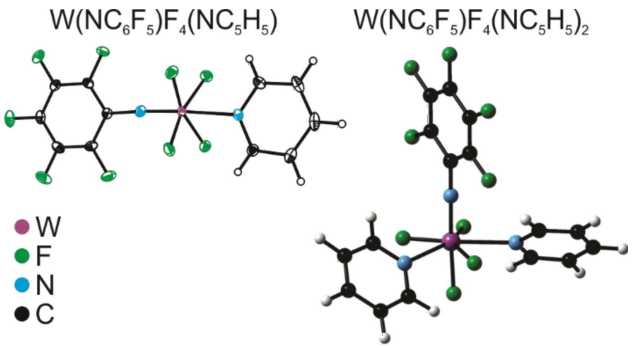

For Table of Contents only.